SUPPLEMENTAL MATERIAL

TABLE OF CONTENTS

ONLINE TABLES

SUPPLEMENTAL REFERENCES

DETAILED ONLINE METHODS

1. LLI populations

The Italian population (comprising 410 LLIs and 553 controls) is described extensively elsewhere.[1] The German sample comprised 1,628 LLIs (age range, 95–110 years; mean age, 98.8 years) and 1,104 younger controls (age range, 60–75 years old; mean age, 66.8 years), and was first described by Nebel et al.[2] The US-American study sample consisted of 1,461 LLIs with an age range of 91–119 years (mean age, 100.8 years) and 526 controls with an age range of 0–35 years (mean age, 28.2 years); these individuals were recruited by Elixir Pharmaceuticals, either directly or through the New England Centenarian Study.[3, 4]

2. Expression of BPIFB4 in different tissues

Expression PCR analysis was performed on a multiple tissue cDNA panel (Clontech) using the following primers for the amplification BPIFB4: fw:CCCAGTATATACCAACGGCAA; rev:ATTTCTCCAGGCTGCAGCT. Amplification results were visualized on an agarose gel with ethidium bromide staining.

3. BPIFB4 RT-PCR analysis in isolated endothelial mature and progenitor cells.

HUVECs were purchased from LONZA and cultured in endothelial basal medium (EBM) supplemented with growth factors (bullet kit) and 2% foetal bovine serum. Endothelial progenitor cells (EPCs) were culture selected from circulating mononuclear cells (MNCs) isolated from peripheral blood (PB) by centrifugation on Histopaque-1077 density medium (Sigma, St. Louis, USA) as we previously described.[5] $CD34^+$ cells were separated from PB-MNCs by magnetic bead-assisted cell sorting (MACS, Miltenyi Biotec, Germany) as we have previously described.[6]

RNA extraction for BPIFB4 gene expression was performed using miRNeasy mini kit (Qiagen) and cDNA synthesis with TaqMan Reverse Transcription Reagent (Applied Biosystems). The quality and concentration of total RNA was determined using the Nanodrop ND1000 Spectrophotometer (Thermo Scientific). PCR primers for gene expression were designed with Primer3 software (fw:GGATATCACCAATGGCATGTT; rev:ATCAGGGCTCCCAGTGTG).

4. Constructs

BPIFB4 cDNA codifies a 575 amino acid protein (identifier: P59827.2) erroneously referred to as an Ile229/Asn281/Phe488/Thr494-BPIFB4 isoform, which retains only the third and fourth amino acid substitutions of the M isoform.[7] The WT- and LAV-BPIFB4 in pRK5 were generated by direct mutagenesis following the manufacturer's instructions (Quik Change Site-Directed Mutagenesis Kit, Agilent Technologies). To obtain the WT isoform, a double nucleotide change was performed to gain Phe488Leu (fw: GACGTGGACACAGAACTCTTGGCCTCATTTTC, rev:GAAAATGAGGCCAAGAGTTCTGTGTCCACGTC) and Thr494Ile (fw:CTTGGCCTCATTTTCCATAGAAGGAGATAAGCTC, rev:GAGCTTATCTCCTTCTATGGAAAATGAGGCCAAG) amino acid shifts; to obtain the LAV-BPIFB4 isoform, a double nucleotide change was performed to achieve amino acid shifts Ile229Val (fw:AGTCTTATTGGCTTCCTGGACGTCGCAGTAGAAGTGAACATCA, rev:TGATGTTCACTTCTACTGCGACGTCCAGGAAGCCAATAAGACT) and Asn281Thr (fw:ATCTCGTGGACAATTTAGTGACCCGAGTCCTGGCCGACGTCCT, rev:AGGACGTCGGCCAGGACTCGGGTCACTAAATTGTCCACGAGAT). To introduce Ser75Ala in the PERK phosphorylation site on BPIFB4, two-step mutagenesis was carried out (fw1:GATCCTTGAGTCCGAGGGAGGCATCAGGGACCTCCGAAAC, rev1:GTTTCGGAGGTCCCTGATGCCTCCCTCGGACTCAAGGATC; fw2:ATCCTTGAGTCCGAGGGAGCCATCAGGGACCTCCGAAA, rev2:TTTCGGAGGTCCCTGATGGCTCCCTCGGACTCAAGGAT). Ser82Asn was introduced to destroy the atypical binding site of the 14-3-3 complex on BPIFB4 (fw:AGGGACCTCCGAAACAATGGCTATCGCAGTGCCG, rev:CGGCACTGCGATAGCCATTGTTTCGGAGGTCCCT). All constructs were sequenced for the BPIFB4 gene.

To obtain BPIFB4 constructs in pAAV2.1 TBG eGFP3 vector, BPIFB4 cDNA was PCR amplified on pRK5 vector[8] with the following primers: AAGCGGCCGCATGCTGCAGCAAAGTGATG for the insertion of

NotI site at 5'end; GCAAGCTTTCATGCGCTCAGCACCAAAAG for the insertion of HindIII site at 3'end. PCR products were purified with Wizard SV Gel and PCR Clean Up System (Promega), digested with NotI and HindIII, and cloned in pAAV2.1 TBG vector replacing the eGFP. All constructs were sequenced for the BPIFB4 gene.

5. Transcriptome analysis

HEK293T cells were grown in culture medium (DMEM, 10% fetal bovine serum, 2 mM L-glutamine, 100 U penicillin/0.1 mg/ml streptomycin) and transfected with pRK5 vector encoding WT-, LAV-, or RV-BPIFB4, or with an empty plasmid, using Lipofectamine 2000 (Life Technologies) according to the manufacturer's protocol, in triplicates. 24 hrs after transfection, cells were serum-starved for 18 hrs and then RNA extracted using the small RNA miRNeasy Mini Kit (Qiagen). The quantity of RNA was determined using a Nanodrop Spectrophotometer, and the quality of RNA, was evaluated by capillary electrophoresis on an Agilent Bioanalyzer 2100 using an RNA nano assay. 1000mg of RNA for each sample were retro-transcript to cDNA and then to cRNA and finally amplified using the Illumina Total Prep RNA amplification Kit (Life Technologies). 750 ng of cRNA of each sample were hybridized with BeadChipIllumina according to the manufacturer's protocol. The fluorescence signals were detected with Illumina iScan. Raw gene expression data were background-subtracted, normalized using the "Rank Invariant" algorithm provided by the Illumina software, and filtered on the basis of negative control beads. Probes were considered detected with p-values ≤ 0.05 in at least one of the samples collected for each cell population. An average expression value for each gene in each population was obtained by merging the values of probes corresponding to the same gene symbol. Complete transcriptome analysis datasets are available in Gene Expression Omnibus (GEO) database (www.ncbi.nlm.nih.gov/geo) in GSE63912.

6. Expression analysis by qPCR

RNA was extracted from cells using the small RNA miRNeasy Mini Kit (Qiagen) and quantified by Nanodrop Spectrophotometer. Genomic DNA was removed by DNase I treatment. Reverse transcription was performed on 1µg of total RNA. Real-time PCR was performed by using the following primers for HSPA6 (fw:GGGGGACAAATGTGAGAAAG; rev:AGAGACAGGGGAGCCACAT), HSPA7 (fw:GGTAAGGCTAACAAGATCACCAA; rev: GGCTTCATGAACCATCCTCT), HSP40 (fw:GGCCTACGACGTGCTCAG; rev: GTGTAGCTGAAAGAGGTACCATTG), HSPA1A (fw:GAAGAAGGTGCTGGACAAGTG; rev:GATGGGGTTACACACCTGCT), mVEGF (fw:TCTCCCAGATCGGTGACAGT; rev:GGGCAGAGCTGAGTGTTAGC), mSOD3 (fw:CCTTCTTGTTCTACGGCTTGC; rev:TCGCCTATCTTCTCAACCAGG), BPIFB4 (fw: GTGGGTGTCTACCTGAGCTTGTA; rev: ACAAGACCCAGCACCACATC), 18S (fw:GTAACCCGTTGAACCCCATT; rev:CCATCCAATCGGTAGTAGCG), with GoTaq PCR Master Mix (Promega), and the results determined with 7900 real-time detection system (Applied Biosystems). Reaction mixtures (15µl) included 10 ng of cDNA and 300 nM concentrations of primers in the reaction buffer and enzyme supplied by the manufacturer. All reactions were performed in triplicate, including negative control samples, which never showed significant threshold cycles (C_T). The relative amounts of the transcripts were determined with 18S rRNA as the reference gene ($[C_{T(\text{gene of interest})} - C_{T(16S)}] = \Delta C_T$).

7. Western blotting

Western blotting was performed on transfected HEK293T, pooled protein extracts from transfected perfused vessels, or from MNCs. Protein extracts were separated on 10% SDS-PAGE at 100V for 1 hr or on 4–12% SDS-PAGE at 100V for 2 hrs and then transferred to a nitrocellulose or PVDF membrane. The membranes were incubated overnight with the following primary antibodies: anti-phospho-EIF2S1 Ser51 (Abcam, rabbit mAb, 1:1000), antiEIF2-alpha (Santa Cruz Biotechnology, mouse mAb, 1:1000), anti-phospho-eNOS Ser1177 (Cell Signaling Technology, rabbit mAb, 1:1000), anti-eNOS (Cell Signaling Technology, mouse mAb, 1:800), anti-BPIFB4 (Abcam, rabbit pAb, 1:200), anti-beta-actin (Cell Signaling Technology, mouse mAb, 1:3000), anti-PKC-alpha phospho-T497 (Abcam, rabbit mAb, 1:10000), anti-PKC-alpha (Abcam, rabbit mAb, 1:1000), anti-SIRT1 phospho-S47 (ImmunoWay Biotechnology, rabbit pAb, 1:500), and anti-SIRT1 (Biorbyt, rabbit pAb, 1:200). After a triple wash, membranes were incubated for 1 or 2 hrs with the secondary antibody (Amersham Life Science, horseradish peroxidase-linked anti-rabbit IgG or anti-mouse IgG, 1:3000). The membranes were then washed four times and specific protein bands were detected with ECL Prime chemiluminescent agents (Amersham Life Science). Western-blot data were analyzed using

ImageJ software (developed by Wayne Rasband, National Institutes of Health, USA) to determine optical density (OD) of the bands. The OD readings of phosphorylated proteins were expressed as a ratio relative to total protein or to beta-actin. All other protein expressions were normalized to beta-actin to account for variations in loading.

A specific antibody for the phosphorylated form of BPIFB4 at serine 75 was generated in collaboration with Areta International (http://www.aretaint.com/), as follows: BalbC mice were immunized with the antigen peptide EGSIRDLRNC (phosphorylated on serine) from the protein BPIFB4 administered intraperitoneally together with Freund's adjuvant (Complete FA at first dose, Incomplete FA at second and third doses, pre-fusion dose without adjuvant). Three days after the pre-fusion dose, spleen cells were fused with myeloma cells (NS0 cells). After a 2-week incubation in hypoxanthine-aminopterin-thymidine selective medium, the hybridoma supernatants were screened for antibody binding activity by ELISA. 4G3 clone was identified as specific for the specific phosphorylated peptide. The 4G3 supernatant was used for our experiments to detect phospho-Ser75 BPIFB4.

8. Co-immunoprecipitation

Forty-eight hours post-transfection, HEK293T cells were harvested and solubilized in lysis buffer (20 mMTris-HCl, pH7.5, 650 mM sodium chloride, 500 mM EDTA, 250 mM EGTA, and Triton X-100). Treatment with GSK2606414 (0.6 μM), was performed for 2h before the harvesting. The cell lysates were cleared at 13,000 rpm for 20 min at 4ºC and the protein concentration of the supernatant was determined with the Bradford Protein Assay (Bio-Rad). 700 μg protein were incubated overnight with 2 μg of anti-GFP (Invitrogen, mouse mAb), anti-14-3-3 (Abcam, mouse mAb), anti-HSP90 (Abcam, mouse mAb), and anti-IgG (Millipore, mouse pAb) for control. The antibody–antigen complexes were precipitated with protein G-linked Sepharose (GE Healthcare) for 4 hr at 4°C and the beads were washed three times with lysis buffer. The denatured co-immunoprecipitation products were resolved with SDS-PAGE, electro-blotted onto PVDF membranes, and hybridized with anti-BPIFB4 (Abcam, rabbit pAb, 1:500).

9. Immunofluorescence and confocal microscopy

HeLa cells were grown in culture medium (DMEM supplemented with 10% fetal bovine serum, 2 mM L-glutamine, 100 U penicillin/0.1 mg/ml streptomycin) in multi-chamber slides and transfected with pRK5 vector encoding WT-, or LAV-BPIFB4, or with an empty plasmid, using Lipofectamine 2000 (Life Technologies) according to the manufacturer's protocol. 24 hr post-transfection, cells were serum-starved for 2 hr, fixed in 4% paraformaldehyde in PBS for 20 min, washed twice in PBS, and permeabilized for 5 min in 0.2% Triton X-100 in PBS. Fixed cells were treated as described.[9] Fixed cells were incubated with anti-14-3-3 (Cell Signaling Technology, rabbit pAb, 1:400) overnight and then with Alexa Fluor 546 secondary antibody (1:1000). Control staining was performed with 2 μg/mL of the vital dye Hoechst 33258 (Sigma Aldrich).

The λ of the two HeNe lasers was set at 543 and at 633 nm. Fluorescence emission was revealed by 560–615 band pass filter for Alexa Fluor 546. Double-staining immunofluorescence images were acquired separately in the red and infrared channels at a resolution of 1024 x 1024 pixels, with the confocal pinhole set to one Airy unit and then saved in TIFF format. Immunofluorescence analysis of 14-3-3 and BPIFB4 was executed under an Olympus BX51 epifluorescence microscope or a Fluoview BX 61 confocal microscope with confocal system FV50 with inserted filter wavelength filters for DAPI (λ_{exc} 405 nm), FITC (λ_{exc} 488 nm), and TRITC (λ_{exc} 546 nm). The fluorescence for the nuclear dye (DAPI channel) and that for the transfected protein (FITC channel) was measured at a single-cell level by a patented cell-segmentation software (Tissue Quest, Wien, Austria).

10. Isolation and characterization of mononuclear cells

DNA was extracted from peripheral blood of healthy subjects (QIAamp DNA blood midi kit, Qiagen) and was genotyped using Taqman probe rs2070325. MNCs were isolated from the peripheral blood of appropriate donors using a density gradient media (Histopaque-1077, Sigma-Aldrich), disrupted in lysis buffer charged with phosphatase inhibitor cocktails (Sigma-Aldrich), and the protein extracts analyzed by Western blotting.

11. EPC migration assay

MNCs were isolated and EPCs enriched as described previously.[10, 11] Antigenic profile was assessed using a FACS Canto flow cytometer and FACS Diva software (Becton, Dickinson and Company). Migration was

performed as described elsewhere.[10, 12, 13] Briefly, cells ($7.5x10^4$) were seeded in the upper chamber of 5 μm pore-size filter-equipped transwell chambers (Corning) coated with fibronectin and allowed to migrate toward SDF-1⟨ (R&D) (100 ng/mL) or vehicle control (bovine serum albumin 1%) for 12 hours at 37°C. Cells migrated to the lower side of filter were counted after nuclear staining with DAPI in 5 random fields at 20X magnification.

12. Ex vivo transfection of mouse vessels and evaluation of vascular reactivity

Second-order branches of the mesenteric arterial tree were removed from C57BL6 mice and transfected as described previously.[14] Briefly, vessels were placed in a Mulvany pressure system filled with Krebs solution supplemented with 20 μg of the pRK5 vector encoding either WT-BPIFB4, LAV-BPIFB4, LAV-$BPIFB4^{mutPERK}$, or LAV-$BPIFB4^{mut14\text{-}3\text{-}3}$, or with an empty plasmid as a negative control. Some vessels were transfected with a *BPIFB4*-siRNA or a scrambled control siRNA. All vessels were perfused at 100 mmHg for 1 hr and then at 60 mmHg for 5 hrs.

The mix of four siRNA (ON-TARGET plus SMART pool l-009125-02-0005, Human C20ORF186) was used in gene silencing. All these fragments are highly specific for human BPIFB4 and three of them map the region from 101 to 242 on BPIFB4 mRNA. There are no related genes in humans with high homology to BPIFB4 so the gene silencing was highly specific.

Vasoconstriction was assessed with 80 mM KCl or with increasing doses of phenylephrine (from 10^{-9} M to 10^{-6} M) in control conditions and after L-NAME exposure (300 μM), and the corresponding values are reported as the percentage of lumen diameter change after drug administration. Responses were tested before and after transfection. Endothelium-dependent and -independent relaxations were assessed by measuring the dilatory responses of mesenteric arteries to cumulative concentrations of acetylcholine (from 10^{-9} M to 10^{-5} M) or nitroglycerine (from 10^{-9} M to 10^{-5} M), respectively, in vessels pre-contracted with U46619 at a dose necessary to obtain a similar level of pre-contraction in each ring (80% of initial KCl-evoked contraction).[15] The maximal contraction evoked by U46619 was considered as the baseline for subsequent evoked vasorelaxations. Acetylcholine vasorelaxation was also tested in the presence of GSK2606414 (0.5 μM), a PERK inhibitor, and SNX5422 (400nM) (Selleckchem, USA), a HSP90 inhibitor. Caution was taken to avoid endothelial damage; functional integrity was reflected by the response to acetylcholine (10^{-6} M).[16]

13. Vector production and purification

Adeno-associated viral vectors were produced at the AAV vector facility of TIGEM, Italy. In brief, 10-layer cell stacks containing 2.2×10^9 of low passage 293 cells were triple-transfected by calcium phosphate with 1000 μg of pAd helper, that contains the adenovirus E2A, E4, and VA RNA helper genes,[17] 520 μg of pAAV2/9 packaging plasmid with AAV rep and cap genes,[18] and 520 μg of pAAVCis. Medium was changed the following day and cells were harvested 3 days after transfection.[19] Cell lysates were purified by two rounds of cesium chloride centrifugation.[20] For each viral preparation, physical titers (GCml-1) were determined by averaging the titer achieved by dot-blot analysis[21] and by PCR quantification using TaqMan[20] (Applied Biosystems, Carlsbad, CA, USA).

14. Infection of hypertensive rats with AAV and measurements of vascular function and blood pressure

Femoral arteries of male spontaneously hypertensive rats (SHR) weighing ~250g were analyzed in this study. The experimental protocol for this project was approved by the Istituto Neurologico Mediterraneo Neuromed, Italy, and complies with NIH guidelines for care and use of laboratory animals. The animals were placed individually in an induction chamber and anesthesia was induced with 5% isoflurane in 100% oxygen with a delivery rate of 5 L/min until loss of righting reflex. After induction, the animals were moved to a homeothermic blanket (N-HB101-S-402) and placed in dorsal recumbence. Anesthesia then was maintained with 1% isoflurane in 100% oxygen with a flow of 1.5 L/min administered by means of a facemask connected to a coaxial circuit (Fluovac anesthetic mask). The procedures replicated typical clinical practice when laboratory mice are anesthetized for surgical procedures. Body temperature was maintained at 37°C with a homeothermic blanket. Animals remained anesthetized for 1 h, after which all animals received 100% oxygen until recovery of righting reflex. Vascular surgery was performed with the aid of a microscope at 2–10X magnification. Femoral arteries were exposed and isolated circumferentially from the inguinal ligament to the knee; all side branches were ligated. To obtain an isolated arterial segment, the superficial femoral

artery was first controlled proximally with two microvascular clips. After temporary clamping of the proximal and distal femoral artery, either 100 µl of saline alone or saline plus AAV-GFP or AAV-LAV-BPIFB4 was infused into the femoral artery and incubated for 15 minutes. Viral titer was 1×10^{13} GC/kg for each experimental condition. After incubation, the distal femoral artery was permanently ligated, and clamps on the proximal femoral artery were removed to restore femoral blood flow. Animals were sacrificed at seven days after surgery and infection. Femoral arteries were excised and were placed on wire system[16] to perform vascular reactivity studies. Blood pressure was evaluated in another experimental series of spontaneously hypertensive rats (11-week-old) by tail-cuff plethysmography for one week as previously described.[16]

15. ELISA quantification of BPIFB4

Quantitative determination of BPIFB4 in serum of animals treated with AAV-LAV BPIFB4 and AAV-GFP was performed with ELISA (code: CSB-EL003694HU, CUSABIO).

16. Immunofluorescence analyses of mesenteric artery

Segments of the mesenteric artery were dissected free of fat and connective tissue from C57BL6 mice injected with AAV-LAV-BPIFB4 and frozen in OCT embedding medium. Frozen sections (10um) were treated with blocking solution (2% donkey serum, 1.5% BSA, 0.5% fish gelatin) for 45 min and immunostained overnight at 4 °C in blocking solution with antibodies anti-BPIFB4 (1:100; Abcam), anti-αSMA-eFluor570 (1:400; eBioscience), sheep anti-Von Willebrand (1:100; Abcam) and revealed with appropriate secondary antibodies (Rhodamine-Red anti-mouse IgG; Jackson ImmunoResearch; Alexa Fluor 488 anti-mouse and anti-sheep IgG; Molecular Probes, Invitrogen). Nuclei were counterstained with DAPI. The images were acquired using a fluorescence (Zeiss Axio Observer A1) microscope with 40X objective.

17. Immunohistochemical analysis from infected mice tissues

Brain, adipose tissue, liver and femur from C57BL6 mice infected with AAV-LAV-BPIFB4 were fixed with 4% PFA solution and routinely processed to paraffin blocks. Tissue slices (2,5 µm) were deparaffinized in xylene and rehydrated in solutions with decreasing alcohol content. Antigen retrieval was conducted by boiling the samples in citrate buffer (sodium citrate 10 mM, 0.05% Tween-20, pH 6) and the endogenous peroxidase activity was blocked with 3% H_2O_2 in methanol for 5 min. The sections were treated with blocking solution (2% donkey serum, 1.5% BSA, and 0.5% fish gelatin) for 45 min and immunostained 1hr at room temperature in blocking solution with primary antibodies anti-BPIFB4 (1:100; Abcam). Immunohistochemistry signals were revealed by incubating the sections with Dako REAL™ EnVision™/HRP, Rabbit/Mouse (ENV) for 25min at room temperature followed by a color reaction using Dako REAL™ DAB+ Chromogen for 5 minutes. The slides were counterstained with Mayer's hematoxylin for 1 min, dehydrated, cleared and mounted.

18. FACS analyses of mice infected vessels

Endohelial cells obtained from C57BL6 mice injected with AAV-GFP and AAV-LAV-BPIFB4 were stained with antibody anti-CD31-FITC (1:100, BD, Biosciences-Pharmigen) at 4°C for 20 min and then permeabilized with cytofix/cytoperm (BD, Biosciences-Pharmigen) at 4°C for 20 min. Subsequently, cells were incubated with primary antibody anti-BPIFB4 (1:100; Abcam) at 4°C for 1 hr and an APC-conjugated anti-mouse secondary antibody (1:200; BioLegend). Analyses of cell populations were performed using a FACS Canto II equipped with FACS Diva software (BD Biosciences).

19. Infection of hindlimb ischemia mice models with AAV and measurement of superficial blood flow and neovascularization

Experiments of this section involving live animals were performed in accordance with the Guide for the Care and Use of Laboratory Animals (The Institute of Laboratory Animal Resources, 1996) and with approval of the British Home Office and the University of Bristol.

Mice were separate to 3 groups and 10 µl $1x10^{11}$ Viral vectors (AAV219-EGFP1966, AAV-LAV- BPIFB4 and AAV-WT-BPIFB4) were injected through the tail vein 16 hours before limb ischemia (n=10 per group). Following anesthesia (2,2,2tribromo ethanol, 0.3mg/kg, i.p.), unilateral limb ischemia was induced in 7-8 weeks old male CD-1 mice (Harlan, UK), using a refined procedure which consists of ligation (with a 7-0 silk suture) in 2 points and electrocoagulation of the upper part of the femoral artery. Mice were then allowed to regain consciousness.

Foot blood flow was measured immediately after ischemia and then at 7, 14 and 21 days (n=10 mice/group) by using a laser Doppler perfusion imaging system (Moor Instrument, UK).
The occurrence of necrotic toes was assessed by daily inspection and recorded. Animals with necrosis extending to the whole foot were sacrificed with an excess of anesthesia.
At 21 days after ischemia, terminally anesthetized mice (n=7 at each time point) were perfused with 10ml PBS and then 10ml 4% paraformaldehyde. Muscle cryosections with thickness of 5μm were used for immunohistochemical analysis unless specified. The capillary and arteriole densities of ischemic adductor muscles were assessed using isolectin-B4 and α-smooth muscle actin (Sigma-Aldrich, UK) staining respectively. Counts of 10 random microscopic fields were averaged and expressed as the number of capillaries and arterioles per mm^2.

20. Evaluation of the modulation in recruitment of total, and short-term and long-term reconstituting LSK cells in the ischemic muscles of AAV injected mice.

In pilot experiments we found that day 3 corresponds to the peak homing time for LSK cells to home into ischemic muscle of mice subjected to femoral artery ligation. Three groups mice (n=5 per group) were injected with 10μl $1x10^{11}$ Viral vectors (AAV219-EGFP1966, AAV-WT-BPIFB4 and AAV-LAV-BPIFB4) through the tail vein, 16 hours before induction limb ischemia The relative abundance of LSK and $CD34^+$LSK cells in PB and ischemic adductor muscles was assessed by multicolor flow cytometry. The following preparatory protocols were applied:

Isolation: LSK cells were also enriched from adductor muscles of mice undergoing limb ischemia. Muscles were harvested, minced with fine scissors and placed into a digest solution of Collagenase A 100 μg/μl (Roche), Dispase II (1X) 2.4 U/ml (Roche), DNase I 10 mg/ml (Roche), $CaCl_2$ 50 mM, $MgCl_2$ 1 M in PBS at 37°C for 1 h, triturated through 40μm diameter nylon mesh, washed with 0.2% BSA + 0.1% DNAse I in PBS.

Analyses: mouse cells were fixed with 2% PFA 10 minutes and washed with ice-cold Hank balanced salt solution containing 0.5% bovine serum albumin and 0.02% sodium azide and blocked with Fc block (Fc, eBioscience anti mouse CD16/32) and stained with antibodies against the following markers: Lineage Mixture Alexa 488 1:100 (mouse CD3e, CD11b, CD45R, Ly-6C/G, TER119, Caltag), Ly6-A/E perCP cy5.5 1:300 (Sca-1, eBioscience), CD117 Alexa780 1:300 (c-Kit, eBioscience), and CD34 Alexa 647 1:100 (eBioscience). Analyses of antigenically defined cell populations were performed using a FACS Canto II equipped with FACS Diva software (BD Biosciences).

21. Statistical analyses

Genetics The reader may refer to Malovini A et al.[1] for details about the statistical methods and procedures applied to the analysis of data deriving from the genome-wide scan. Association tests within the replication cohorts were performed by logistic regression, assuming the genetic model hypothesized by the genome-wide scan. Logistic regression was implemented in the "base" package of the R statistical software[22] (http://www.R-project.org). Meta-analysis was performed by the *metabin* function implemented in the R package called "meta" (http://www.R-project.org, http://cran.rproject.org/web/packages/meta/index.html). Statistical power calculations were performed by the QUANTO software tool (http://biostats.usc.edu/Quanto.html), setting the prevalence of longevity trait in the general population as ~ 1/10,000, as reported by Ferrario et al.[23]

Haplotype analysis SNPs showing pairwise correlation $r^2<0.80$ in the Italian cohort were identified by the PLINK software tool[24] (command: --indep-pairwise 1500 150 0.8). Positional and functional annotations of the identified SNPs were performed by the SNPNexus on-line tool (http://www.snp-nexus.org/).

BPIFB4 RT-PCR analysis in isolated endothelial mature and progenitor cells Each Real time PCR reaction was performed in triplicate, and relative expression of mRNAs was calculated by the $2^{-\Delta\Delta Ct}$ method[25] using 18S ribosomal RNA as endogenous control. Statistical analysis was performed using Mann Whitney test. Data presented as mean±SEM.

EPC migration To assess migration to the chemoattractant (SDF-1⟨), number of migrated cells with or without SDF-1⟨ were compared using Student's t-test via GraphPad Prism Software, version 5.0. Values are expressed as mean ± SE.

Expression analyses Expression data are indicatedas mean ± SEM. One-way ANOVA statistics were calculated (GraphPad Prism Software, version 5.0).
Transcriptome and GO analysis Differential expression *P*-values for the detected transcripts were computed with a permutation-based test that builds a null distribution of the fold-change values by randomly shuffling the samples' labels.[26] Modulated genes were selected using a *P*-value cut off of 0.01. Enrichment of a priori-defined gene sets was performed with the hypergeometric test and enriched GO categories with FDR corrected *P*-values ≤ 0.01 were selected with statistical and bioinformatics functions implemented in the Orange Data Mining Suite (http://orange.biolab.si/).
Western Blotting analysis Densitometry data were analyzed with Student's t-test or two-way ANOVA, as appropriate, using a dedicated software (GraphPad Prism Software, version 5.0).
Colocalization data Unpaired Student's t-test was used to compare the percentage of co-localization among the three BPIFB4 variants and nuclear area stained by Hoechst 33258 and to compare the number of co-localizing pixels of the 14-3-3 protein and WT-, and LAV-BPIFB4 signals.
MNC data Unpaired Student's t-test was used to compare the mean (± SEM) of the OD data about the wild-type, homozygous and the heterozygous carriers of the rs2070325 variation.
Ex vivo data Vessel reactivity results are given as mean ± standard error of mean (SEM). Data were analyzed with Student's t-test or two-way ANOVA followed by Bonferroni post-hoc analysis, as appropriate, using a dedicated software (GraphPad Prism Software, version 5.0).
In vivo data Measurements of mice and rat blood pressure are given as mean ± SEM. Data were analyzed with ANOVA, using a dedicated software.
Unpaired Student's t-test was used to compare the amount of cell fractions in the ischemic muscles of AAV injected mice. Values are mean ± SE.
Values of blood flow recovery were compared using unpaired Student's t-test. Values are mean ± SE.
Capillary and arteriole density data were analysed using unpaired Student's t-test. Values are mean ± SE. (GraphPad Prism Software, version 5.0).
ELISA data Unpaired Student's t-test was used to compare the colorimetric values of enzymatic reaction of ELISA kit from controls and centenarians groups.

22. Declaration of ethical approval

The study protocol for the German population was approved by the Ethics Committee of University Hospital Schleswig–Holstein (Campus Kiel), Germany, and local data protection authorities. The US-American study samples were recruited by Elixir Pharmaceuticals, either directly or through the New England Centenarian Study. The study protocol was approved by the Boston Medical Center's Institutional Review Board and by the Western Institutional Review Board.

ONLINE TEXT

Online Text I. The Southern Italian Centenarian study

We tested nearly 298,714 SNPs in 410 LLIs (age range, 90–109 years; mean age, 96.6 years) and 553 young controls (age range, 18–48 years; mean age, 33.0 years), and found 67 potential longevity-associated variants (genomic control adjusted P <1x10^{-4} under allelic, dominant, or recessive genetic models).[1] One SNP (*CAMKIV*-rs10491334), already known to be associated with diastolic blood pressure, was chosen for further study and was found to be associated with longevity also in an independent replication cohort. The other variants remained to be validated.

Online Text II. German and US study populations

The German sample comprised 1,628 LLIs (age range, 95–110 years; mean age, 98.8 years) and 1,104 younger controls (age range, 60–75 years old; mean age, 66.8 years), and was first described by Nebel et al.[2] The study protocol was approved by the Ethics Committee of University Hospital Schleswig–Holstein (Campus Kiel), Germany, and local data protection authorities. The US-American study sample consisted of 1,461 LLIs with an age range of 91–119 years (mean age, 100.8 years) and 526 controls with an age range of 0–35 years (mean age, 28.2 years); these individuals were recruited by Elixir Pharmaceuticals, either directly or through the New England Centenarian Study.[3, 4] The study protocol was approved by the Boston Medical Center's Institutional Review Board and by the Western Institutional Review Board.

Online Text III. Meta-analysis of rs2070325 and statistical power calculations

rs2070325 did not deviate significantly from the Hardy–Weinberg equilibrium in the control populations (P >0.001). Genotype counts of rs2070325 stratified by case/control condition are reported in **Online Table II**.

No statistically significant heterogeneity between the ORs estimated for the two populations was detected (Q-statistic, P>0.05; heterogeneity index, I^2 = 0%). Effect sizes were then combined assuming a fixed effects model (3,060 LLIs and 1,609 controls: OR = 1.49; 95% CI = 1.22–1.81; P = 7.59 x 10^{-5}).

Finally, fixed effects meta-analysis of the screening and replication sets (Q-statistic, P = 0.12; heterogeneity index, I^2 = 52.6%) showed a significant association even after correction for multiple testing, based on the Bonferroni correction on 155,456 SNPs showing pairwise r^2<0.8 in the SICS cohort (3,464 LLIs and 2,160 controls; OR = 1.61; 95% CI = 1.34-1.92; P= 2.4 x 10^{-7}).

The significance threshold for identifying statistically significant associations when combining the effect sizes observed in the screening and replication cohorts was identified based on the Bonferroni correction on 155,456 SNPs showing pairwise r^2<0.8 in the SICS cohort (α = 0.05 / 155,456; P < 3.22 x 10^{-7}).

Power calculations were performed according to the following settings and scenarios.

- **Screening cohort.** Results from statistical power calculations showed that the screening analysis was sufficiently powered (>0.85) to detect the effect observed for rs2070325 in the SICS cohort (OR = 2.42), according to: i) the sample size defining the screening cohort (410 LLIs vs. 553 controls); ii) the significance threshold adopted (P<0.0001); iii) the genetic model tested (recessive); and iv) the MAF observed (MAF = 0.35). Results are graphically represented in **Online Figure I**.
- **Combined replication cohorts**. Similarly, our analysis had sufficient statistical power to detect the effects observed for rs2070325 when combining the effect sizes corresponding to the two replication cohorts (power >0.90 in detecting OR = 1.49; P = 7.59 x 10^{-5}, according to: i) the sample size reached by the replication cohorts combined [3,060 LLIs vs. 1,609 controls]; ii) the significance threshold adopted [P< 0.05]; iii) the genetic model tested [recessive]; and iv) the MAF observed [MAF = 0.35]).
- **Combined screening and replication cohorts**. Finally, the statistical power reached when combining the screening and the two replication cohorts (3,464 LLIs vs. 2,160 controls) was >0.80 in detecting OR = 1.6 observed for rs2070325, according to: i) the sample size defining the screening cohort (3,464 LLIs vs. 2,160 controls); ii) the significance threshold adopted (P < 3.22 x 10^{-7}); iii) the genetic model tested (recessive); and iv) the MAF observed (MAF = 0.35).

Online Text IV. Haplotype analyses of the *BPIFB4* locus

Analysis of the haplotype distribution in 960 Caucasian individuals revealed the presence of a major allele (allele frequency, 66%) carrying the combination AACT and codifying for the wild-type (WT) Ile229/Asn281/Leu488/Ile494-BPIFB4 isoform, and a minor allele (allele frequency, 29.5%) carrying the combination GCTC and codifying for the longevity associated variant (LAV) Val229/Thr281/Phe488/Thr494-BPIFB4 isoform. A rare variant (RV), found in <2% of chromosomes, harbored only the latter two substitutions.

Online Text V. Expression of BPIFB4 in different tissues

Further analysis of BPIFB4 gene expression was assessed with RT-PCR using a commercial panel of human cDNAs (Clontech) from different tissues. We found clear expression in testis and spleen. We also interrogated different tissues and cell lines, detecting BPIFB4 expression in endothelial progenitor cells (EPCs) cultured from MNCs on fibronectin, embryonic stem (ES) cells, induced pluripotent stem (iPS) cells (but not in their originating fibroblasts), and human hypertrophic heart (in which fetal genes are re-activated) and fetal (but not in adult) heart (**Online Figure II**).

We next analyzed human umbilical vein cells (HUVECs), EPCs, circulating $CD34^+$ cells, and total MNCs in LLIs. Of note, we found that EPCs and $CD34^+$ cells had enriched expression of BPIFB4 RNA (**Online Figure IIIA**).

Online Text VI. BPIFB4 isoforms activate adaptive stress responses and proteostasis

Genome-wide transcriptional profiling indicates that BPIFB4 induces the activation of heat shock factor (HSF)1-inducible heat-shock proteins (HSPs), such as HSPA6, HSPA7, HSP40, HSPA1A, HSPB1, and HSPA9, with an increment from 4 to 50 times (**Online Figure V** and **Online Tables III–VI**). We also observed significant up-regulation of the protein translation machinery and of ribosomal biogenesis (**Online Figure VIA** and **Online Tables VI, VII**). Among the many transcripts up-regulated by BPIFB4 isoform overexpression, there was a highly significant enrichment in H/ACA RNAs essential for ribosomal RNA pseudouridylation (snoRNAs) and of spliceosomal small nuclear RNAs (scaRNAs) (**Online Tables III–VI**). The most interesting among the up-regulated scaRNAs is scaRNA19, or TERC, the malfunctioning of which brings to telomere shortening and premature aging in congenital dyskeratosis.[27] Importantly, genes transcribing exosomal mRNAs released by stressed endothelial cells were significantly up-regulated by the different BPIFB4 isoforms[28] (**Online Figure VIA** and **Online Tables III–VI**). Thus, transcriptome analysis strengthens the notion of a role for BPIFB4 in stress adaptation *via* the exosomal machinery.

Online Text VII. LAV-BPIFB4 is more cytoplasmic and forms a complex with 14-3-3 more efficiently than WT-BPIFB4

HeLa cells, characterized by an abundant cytoplasm, were selected for colocalization experiments of the different BPIFB4 isoforms with subcellular compartments/organelles. A different pattern of nuclear/cytoplasmic distribution between WT- and LAV-BPIFB4 was the first, and most evident, difference. In cells expressing WT-BPIFB4, a high percentage of protein overlapped with the nuclear marker Hoechst 33258 (left panel, white arrows), LAV-BPIFB4 had a prevalent cytoplasmic distribution (right panel, red arrows), (**Online Figure VIIIA**). Images were supported by statistical analysis on % of GFP (i.e., BPIFB4) colocalizing with the nuclear stain Hoechst 33258 (**Online Figure VIIIB**).

The peculiar distribution of the BPIFB4 isoforms was also reflected in different profiles of colocalization with protein 14-3-3, whose expression is predominantly cytoplasmic. As clearly observable in highly magnified images (**Online Figure IXA**), BPIFB4 and 14-3-3 colocalized especially when HeLa cells were transfected with LAV-BPIFB4 (right panel). In agreement, co-immunoprecipitation experiments indicate the presence of a BPIFB4–14-3-3 complex when cells were transfected with LAV-BPIFB4, while no detectable co-immunoprecipitation was observed when cells were transfected with WT-BPIFB4 (**Online Figure IX**).

Online Text VIII. Effect of eNOS inhibition on the action of LAV-BPIFB4

Acetylcholine-evoked vasorelaxation in resistance vessels depends on the action of various mediators, such as eNOS, prostanoids and endothelium-derived-hyperpolarizing factor (EDHF); the effect of each of these factors can be restricted by higher amounts of another.[29] Based on this premise and on the above observations, we inhibited eNOS with N^G-nitro-L-arginine methyl ester (L-NAME) in order to clarify whether increased vasorelaxation was effectively due to eNOS-dependent NO production in LAV-BPIFB4-expressing vessels. We found that eNOS inhibition produced more pronounced reduction of acetylcholine-evoked vasorelaxation when LAV-BPIFB4 was expressed (**Online Figure X**). This effect could be explained by higher concentrations of NO reducing the availability of the other acetylcholine vasorelaxation mediators (**Online Figure X**).

Online Text IX. Characterization of AAV injection effects on LAV-BPIFB4 expression

Data from immunohistochemistry studies show localization of BPIFB4 in vascular endothelial and smooth muscle cells of mice injected with AAV-LAV-BPIFB4 (**Online Figure XVIII**). Additionally, we report new results on quantification of BPIFB4-positive vascular cells, indicating increased level of expression in $CD31^+$/endothelial cells of mice intra-arterially injected with AAV-LAV-BPIFB4 as compared to mice injected with AAV-GFP (12.7±3.8 vs. 3.7±0.5%; P=0.01). Furthermore, AAV-LAV-BPIFB4 infection induced BPIFB4 overexpression in femoral bone marrow, brain, adipose tissue, and endothelium, but not in liver as assessed by immunohistochemistry (**Online Figure XIXA**). No differences were detected in AAV-LAV-BPIFB4 versus AAV-GFP infected rat serum (507± 92 vs 551±56 pg/mL P=0.339) and MNCs (**Online Figure XIXB**) — as measured by ELISA and western blot, respectively. Thus, infection with AAV-LAV-BPIFB4 induced overexpression of the transgenic protein in endothelial cells of two and half-folds, as calculated by western blot densitometry analysis (**Figure 4 and 5**) as well as in different organs of the body. Similar to what observed with intra-arterial injection, intra-venous delivery of AAV-LAV-BPIFB4 increased the abundance of $CD31^+$/$BPIFB4^+$ endothelial cells as compared to AAV-GFP (11.0±3.1 vs. 5.3±2.9 %; P=0.08). We also measured the expression of the transgene in the limb ischemia model, where the vector was delivered through the tail vein. We found that the transgenic protein is localized in capillaries and small arterioles, but not in skeletal myocytes, suggesting that accelerated healing is driven by vascular expression of the transgene (**Online Figure XXVI**).

ONLINE FIGURES

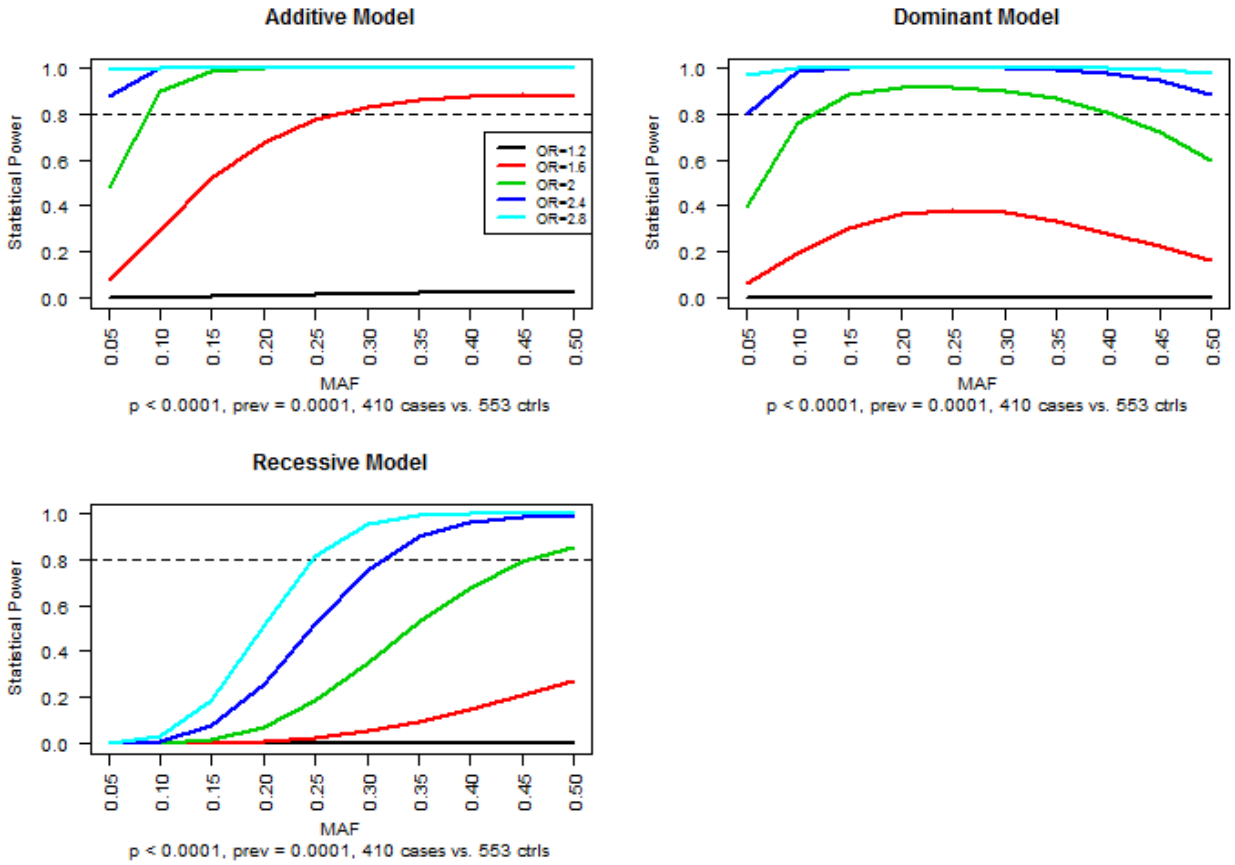

Online Figure I. Statistical power calculations for the screening set.
Each plot reports the results from statistical power calculations according to the additive, dominant and recessive models respectively. The x-axis of each plot reports the minor allele frequency, while the y-axis reports the corresponding statistical power defined according to different ORs (ranging from 1.2 to 2.8), and highlighted with different colors. The horizontal dashed line corresponds to statistical power = 0.8. Statistical power analyses were based on: i) the sample size defining the screening cohort (410 LLIs vs. 553 controls); ii) prevalence of longevity in the general population (~ 1/10,000)[23]; and iii) significance threshold (P<0.0001).

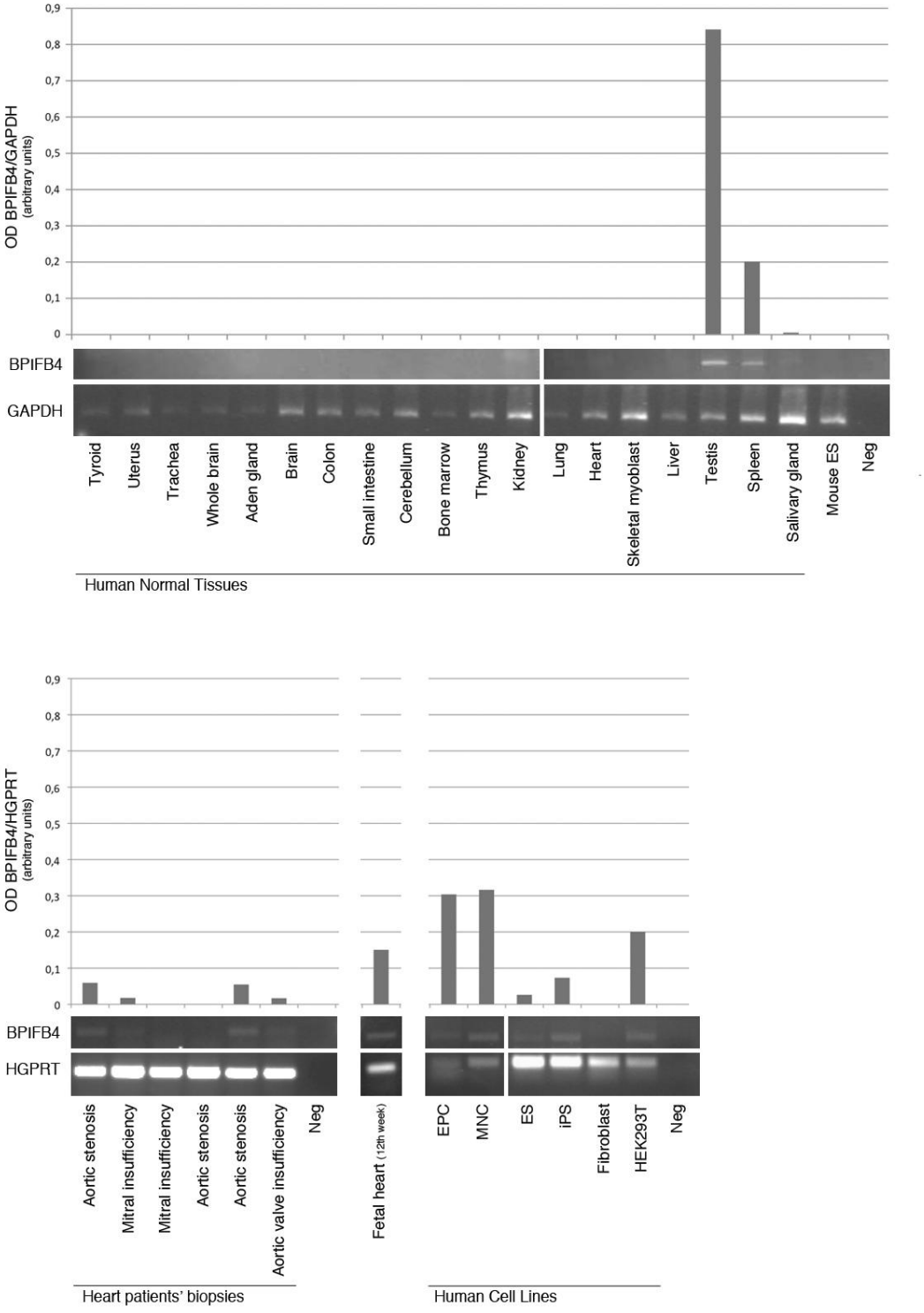

Online Figure II. Expression of BPIFB4 in different tissues.
The image shows the expression of *BPIFB4* and housekeeping genes (*GAPDH* or *HGPRT*) in different tissues (under physiological or pathological conditions) and cell lines by PCR amplification and visualization by agarose gel with ethidium bromide staining. Graphs show optical density values of BPIFB4 expression after normalization vs the housekeeping genes.

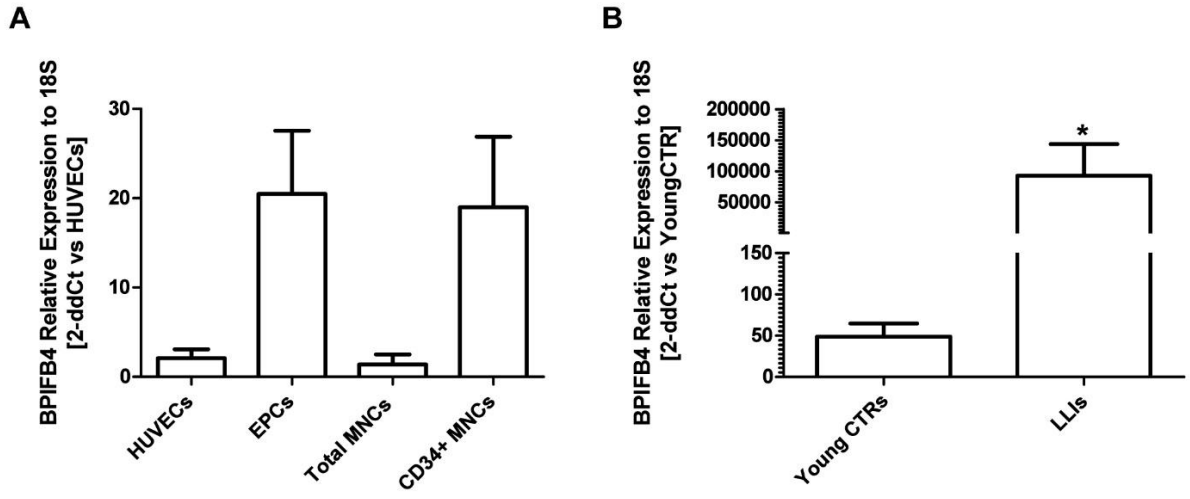

Online Figure III. *BPIFB4* is expressed by mature endothelial and progenitor cells
Graphs of average RT-PCR data showing BPIFB4 mRNA relative expression in **A,** human umbilical vein cells (HUVECs), culture-selected endothelial progenitor cells (EPCs), total peripheral blood mononuclear cells (Total MNCs), and magnetic bead-assisted sorted $CD34^+$ MNCs (N=3), and **B**, $CD34^+$ MNCs from young control volunteers (N=11, age=35±6 years) and LLIs (N=16, age=97±2 years). *, *P*=0.028 vs. CTRs (Mann Whitney test). Data presented as mean±SEM.

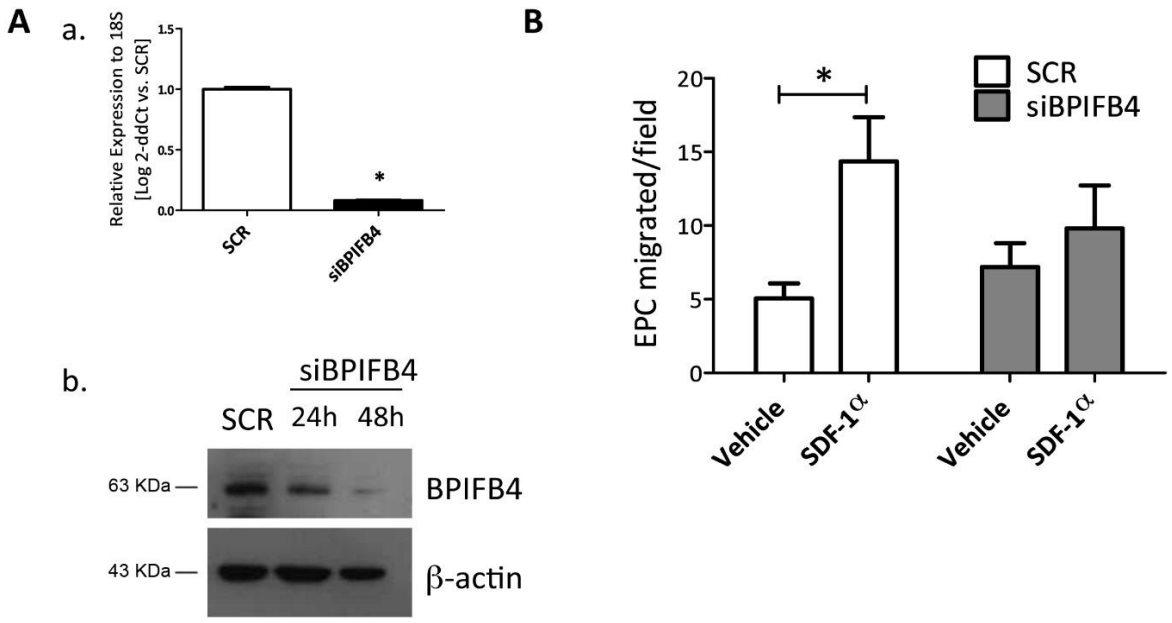

Online Figure IV. Silencing BPIFB4 inhibits *in vitro* migration of endothelial progenitor cells (EPCs). Human EPCs were enriched by selective culture on fibronectin from peripheral blood MNCs. Cells were transfected with siBPIFB4 or scramble (SCR) negative control (both from Dharmacon). **A) a,** BPIFB4 Real Time PCR PC after 48 hours siRNA transfection showing significant inhibition of RNA levels. Data are from one donor assayed in duplicate. * P<0.05 vs. SCR. **b,** Representative Western blot showing effective BPIFB4 protein silencing. **B)** EPCs treated for 48 hours with siBPIFB4 were tested *in vitro* for their ability to migrate along a gradient of the chemoattractant SDF-1 or vehicle. SCR-treated EPCs show significant migration that is blocked when BPIFB4 is silenced. Bar graph shows average migrated cells from 4 independent healthy donors assayed in duplicate wells ±SE. * P<0.05 vs. vehicle.

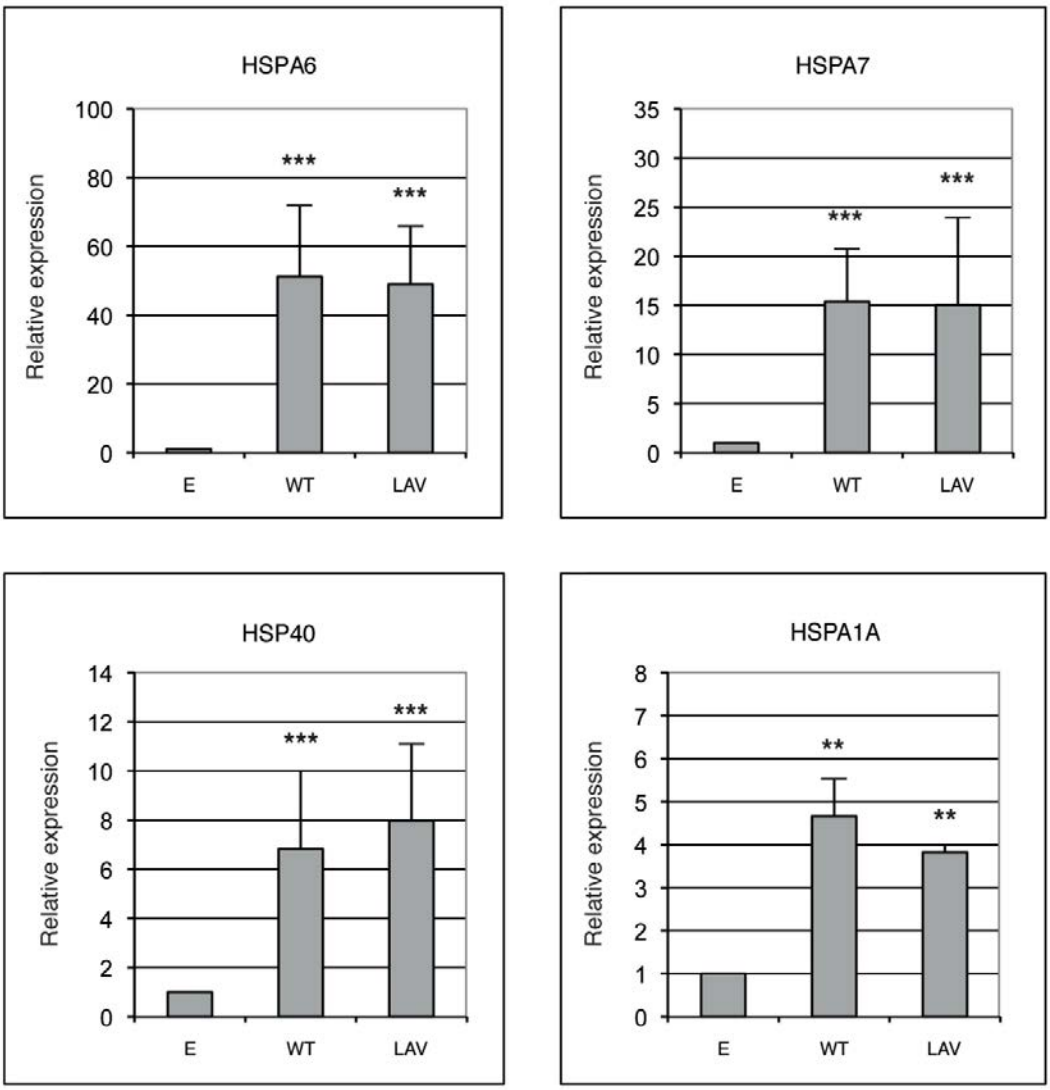

Online Figure V. Enhanced expression of heat shock proteins following forced expression of BPIFB4 isoforms.

Histograms of the relative expression of HSPs in HEK293T cells transfected with empty plasmid (E) or with plasmids carrying WT- or LAV-BPIFB4. Means±SEM; HSPA6 N=4; HSPA7 N=6; HSP40 N=6; HSPA1A N=3.**P<0.01; ***P<0.001 (ANOVA).

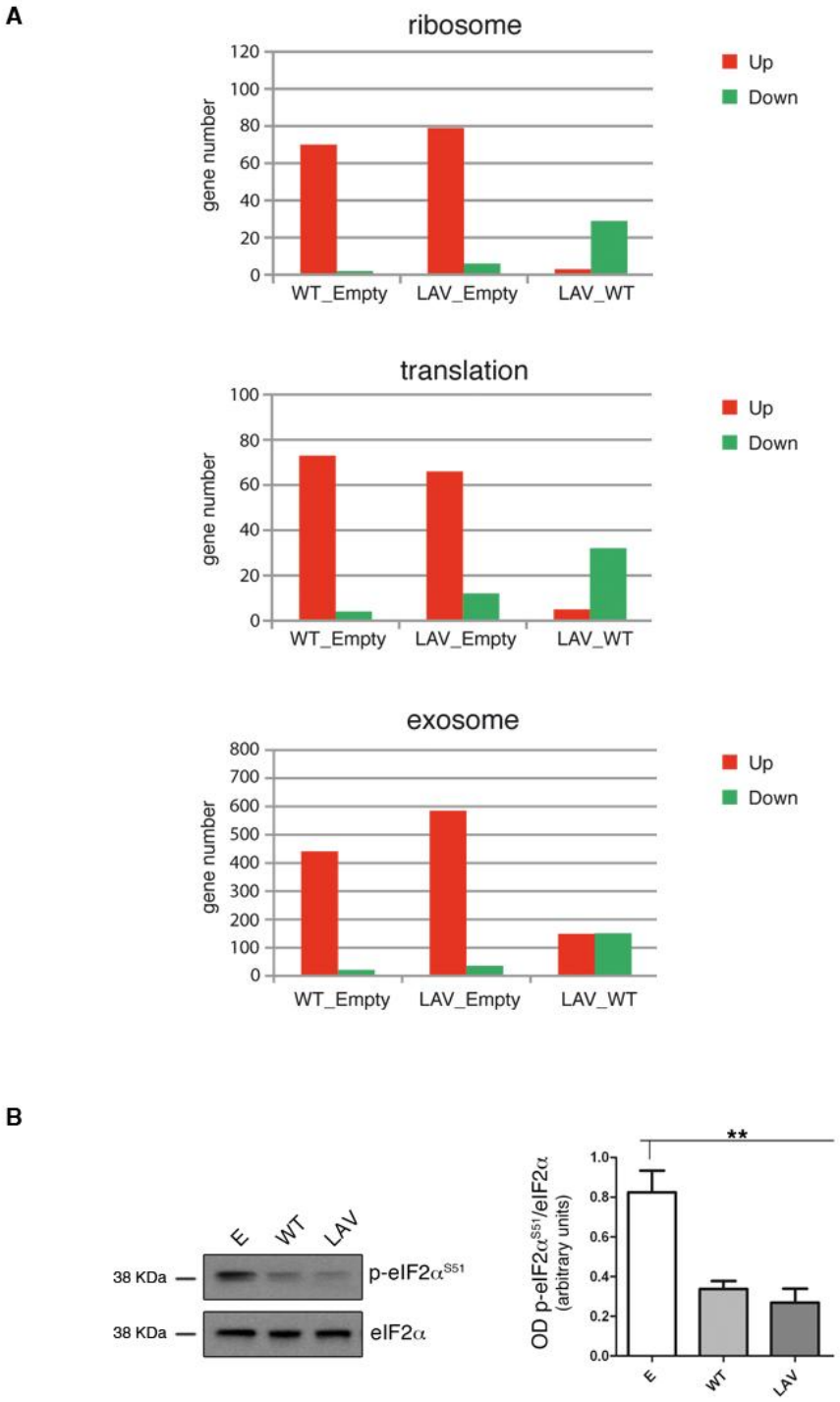

Online Figure VI. Transcriptional profiling and eIF2alpha analysis of cells transfected with BPIFB4 isoforms.

A, Graphs of Gene Ontology categories with the amount of differentially up-regulated (red bars) and down-regulated (green bars) genes in the indicated comparisons of expression profiles of HEK293T cells transfected with the different plasmids. Empty, empty vector; WT, wild-type BPIFB4; LAV, longevity-associated variant of BPIFB4. See **Online Table V** for statistics. **B,** Representative Western blot of the reduced phosphorylation of eIF2alpha at Ser51 after transfection with BPIFB4 isoforms. Right panel shows densitometry and statistical analyses (N=3, ANOVA; **, P<0.01).

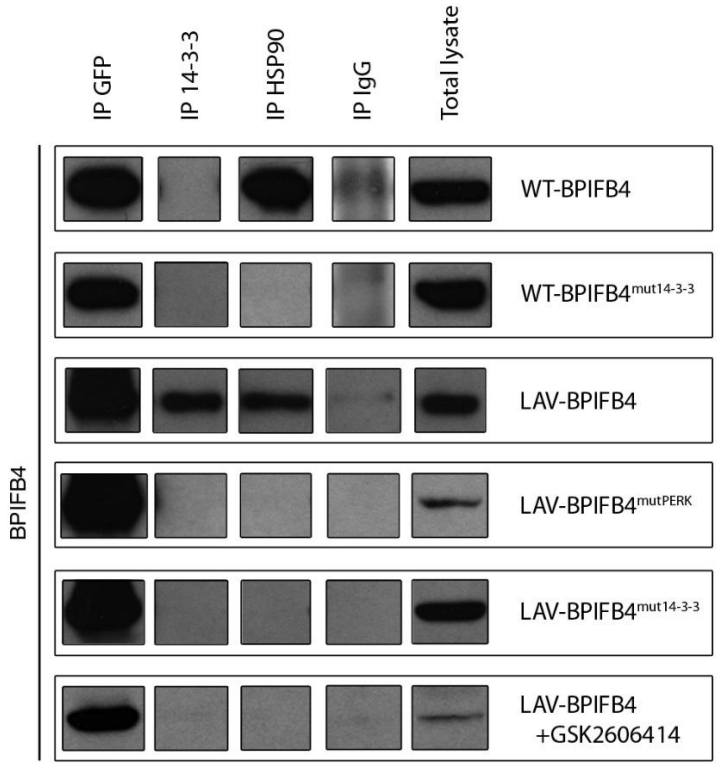

Online Figure VII. Co-immunoprecipitation of BPIFB4, 14-3-3 and HSP90 in HEK293T cells.
Co-immunoprecipitation of BPIFB4 with 14-3-3 and HSP90 in extracts of HEK293T cells transfected with plasmids carrying WT-BPIFB4, WT-BPIFB4 with a Ser82Asn (WT-BPIFB4$^{mut14\text{-}3\text{-}3}$) variation, LAV-BPIFB4, or LAV-BPIFB4 with a Ser75Ala (LAV-BPIFB4^{mutPERK}) or a Ser82Asn (LAV-BPIFB4$^{mut14\text{-}3\text{-}3}$) variation, or LAV-BPIFB4 treated with PERK inhibitor GSK2606414. Co-immunoprecipitation with anti-GFP indicates the presence of BPIFB4 because the plasmids encoded for fusion proteins. IgG and total lysate lanes were used as controls.

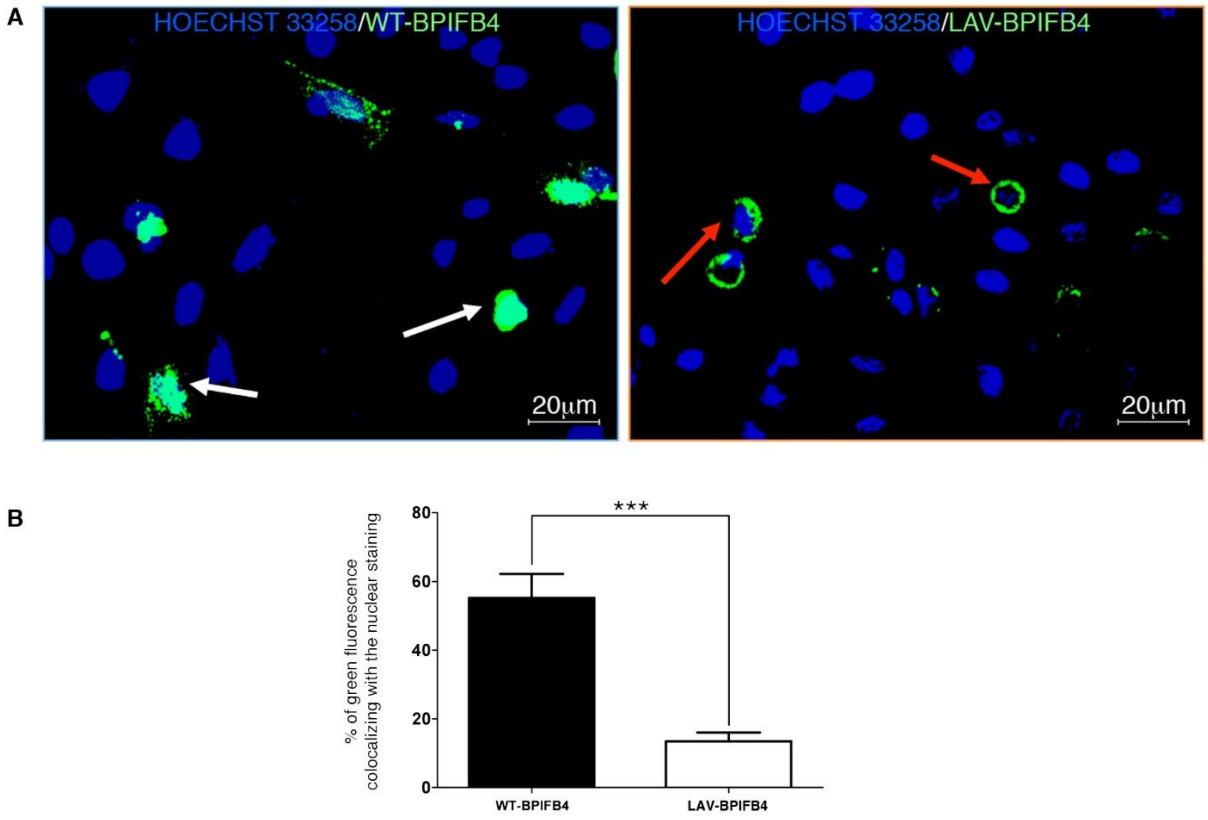

Online Figure VIII. Subcellular localization of BPIFB4 and its isoforms in transfected HeLa cells.
A, Representative panels showing: in light green the profile of expression of WT-BPIFB4 (left) and LAV-BPIFB4 (right); in blue the nuclear marker Hoechst 33258. White arrows indicate nuclear distribution of BPIFB4 protein, while red arrows indicate cytoplasmic distribution. **B**, Histogram of percentage co-localization between the nuclear marker Hoechst 33258 and WT- and LAV-BPIFB4. Data are expressed as mean ± SEM; N=18. ***P*<0.01; ****P*<0.001 (Student's t-test). Overall, these images point to a shift in the localization of BPIFB4 from mainly nuclear (WT isoform) to cytoplasmic (LAV isoform).

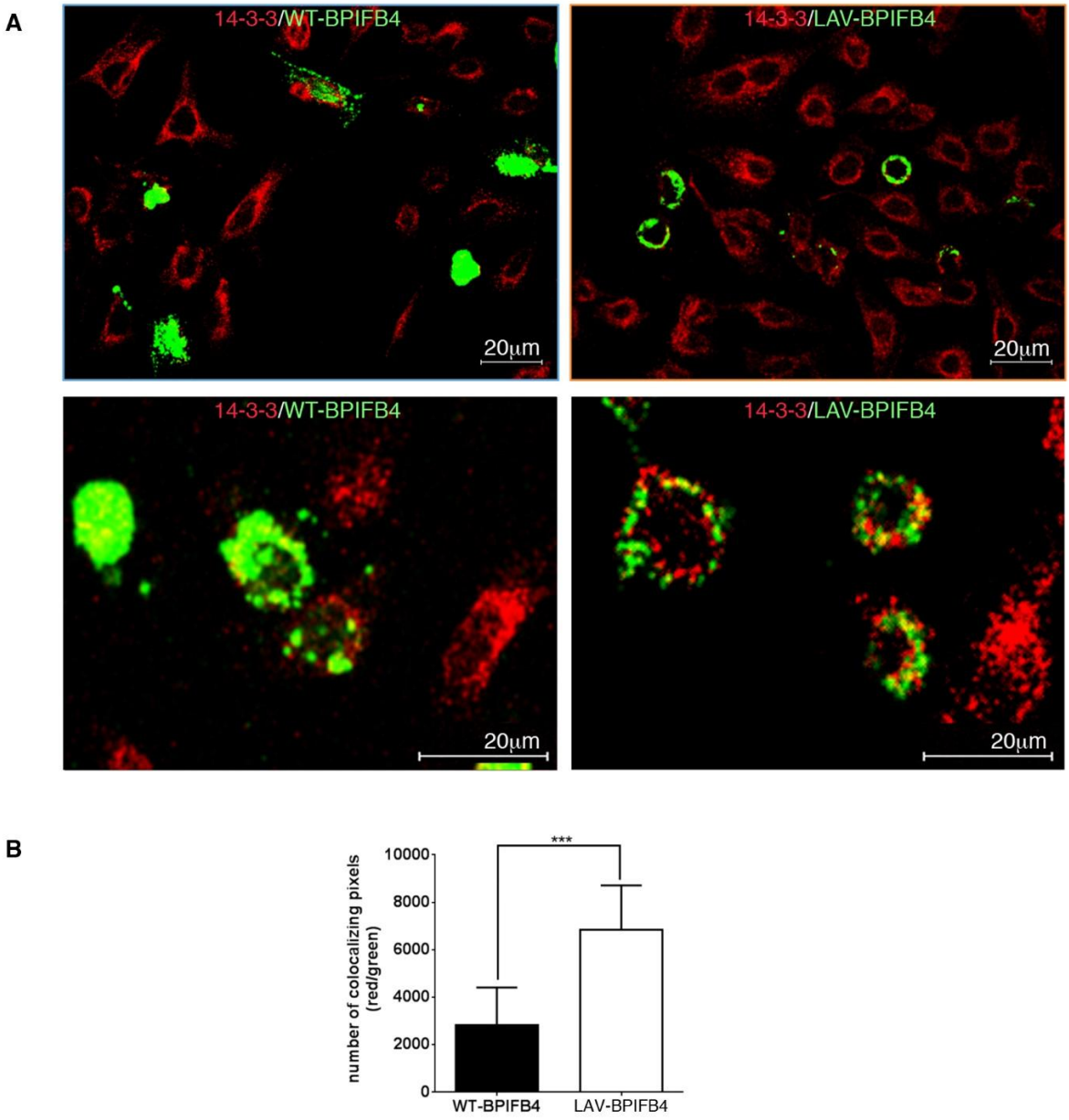

Online Figure IX. Co-localization of BPIFB4 and its mutated form with 14-3-3.
A, Representative merged immunostaining images of the signal from the BPIFB4 isoforms (green) and that from 14-3-3 protein (red). The LAV-BPIFB4 signal co-localizes with that of 14-3-3 (yellow signal). **B**, Histogram of number of co-localizing pixels of the 14-3-3 protein signal and WT- and LAV-BPIFB4 signals. Data are expressed as mean ± SEM; N=12. ****P*<0.001 (Student's t-test).

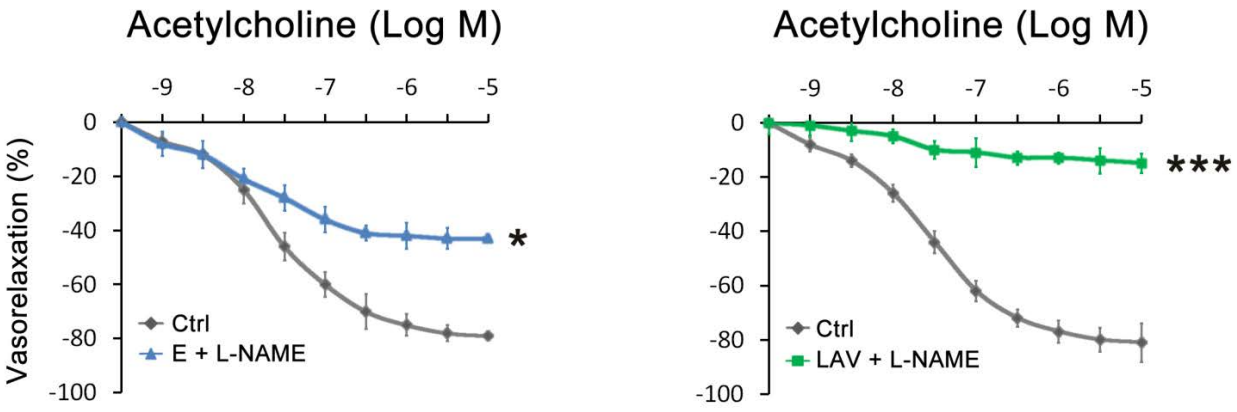

Online Figure X. L-NAME inhibits acetylcholine-induced vasorelaxation of LAV-BPIFB4-transfected vessels.

Dose–response curve to acetylcholine in *ex vivo* C57BL/6 mouse mesenteric arteries untreated (Ctrl) or treated with N^G-nitro-L-arginine methyl ester (L-NAME, 300µM), an eNOS inhibitor, and transfected with empty vector (E, on the left) or with LAV-BPIFB4 plasmid (on the right). The blockade of NO production by L-NAME in LAV-BPIFB4-expressing vessels evoked a more pronounced inhibition of acetylcholine-mediated vasorelaxation compared with that of vessels transfected with an empty plasmid, indicating the presence of a higher NO concentration in the former. Values given as mean ± SEM. N=7; **P* <0.05; ****P* <0.001 (Student's t-test).

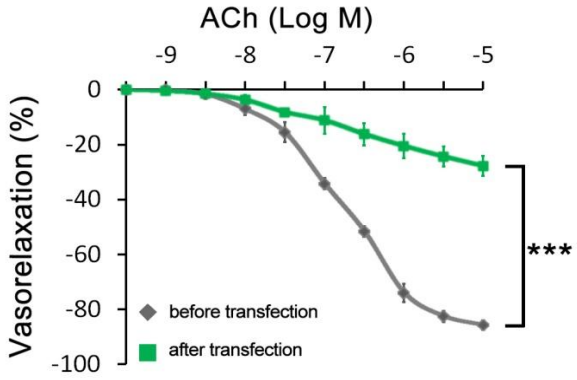

Online Figure XI. Mutation at serine 82 of wild type BPIFB4 (WT-BPIFB4$^{mut14\text{-}3\text{-}3}$) inhibits acetylcholine-mediated vasorelaxation.

The vascular response of *ex vivo* mouse mesenteric arteries to acetylcholine (ACh), before ( ) and after ( ) transfection with WT-BPIFB4$^{mut14\text{-}3\text{-}3}$. Values given as means ± SEM. N=4 experiments per group. *** $P<0.001$ (ANOVA).

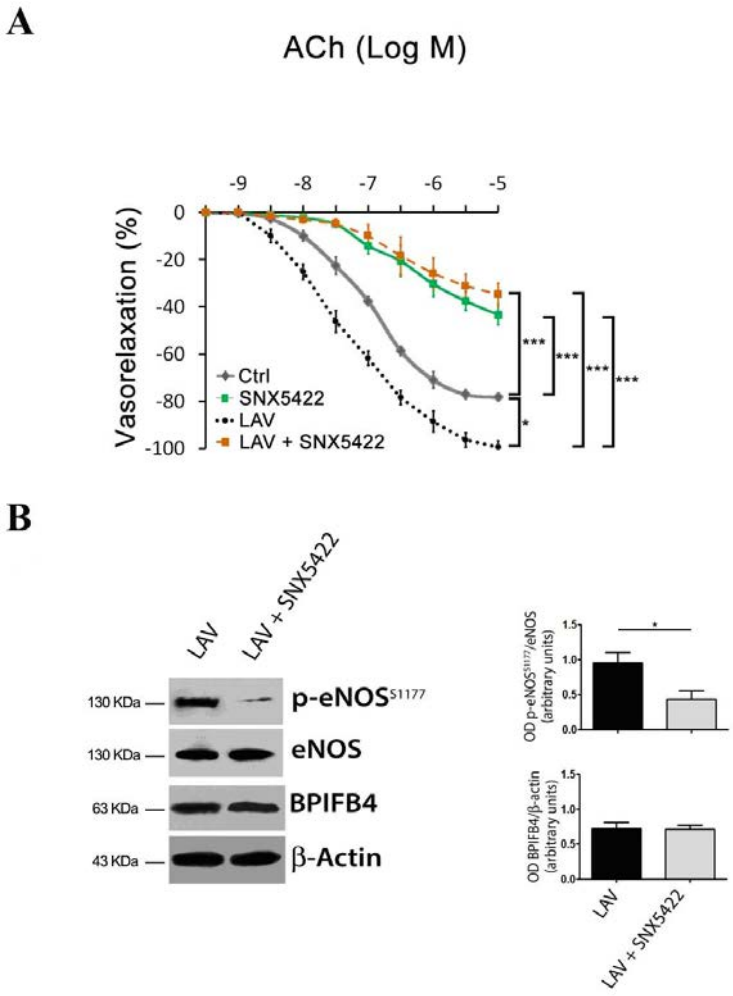

Online Figure XII. The HSP90 inhibitor SNX5422 blunts LAV-BPIFB4-mediated enhancement of vasorelaxation and eNOS activation in mesenteric arteries.

A, The vascular response of *ex vivo* mouse mesenteric arteries to acetylcholine (ACh), before transfection ( ), after treatment with SNX5422 (400nM) ( ), after transfection with LAV-BPIFB4 ( ) and after transfection with LAV-BPIFB4 plus SNX5422 ( ). Values are given as mean ± SEM. N=4 experiments per group. **P*<0.05; ****P*<0.001 (ANOVA). **B,** Western blot of four pooled experiments on mesenteric arteries of *ex vivo* mouse transfected with LAV-BPIFB4 or LAV-BPIFB4 plus SNX5422. Right graphs show quantification of eNOS phosphorylation and BPIFB4. Values are means±SEM, N=2 pools of experiments. Statistic was performed using ANOVA; ***P* <0.01.

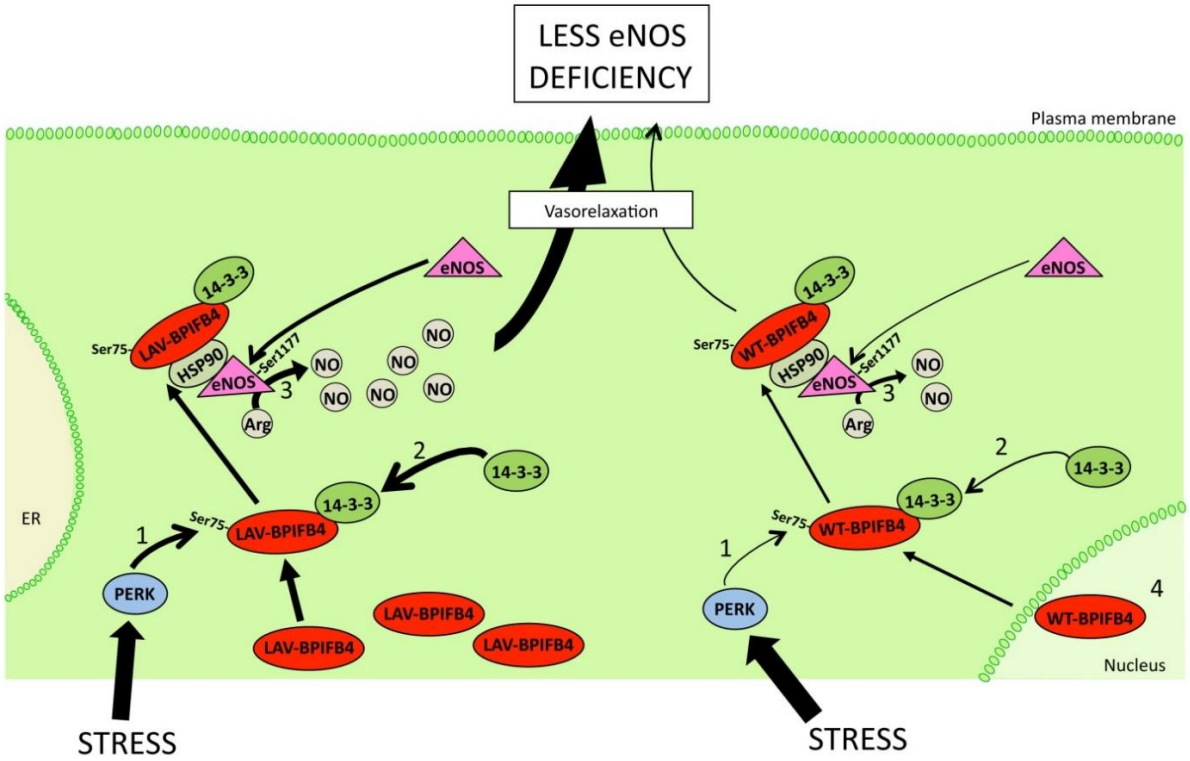

Online Figure XIII. Schematic representation of the hypothetical mechanism of action of LAV-BPIFB4 (on the left) and of WT-BPIFB4 (on the right).
Cellular stress, such as mechanical stress, induces protein kinase RNA-like endoplasmic reticulum kinase (PERK) phosphorylation of both LAV- and WT-BPIFB4, with more efficiency for the LAV-isoform (1). LAV-BPIFB4 binds to 14-3-3 more efficiently than WT-BPIFB4 (2). Endothelial nitric oxide synthase (eNOS) is activated by BPIFB4/14-3-3/heat shock protein (HSP)90-mediated mechanisms to increase the production of nitric oxide (NO) from L-arginine (Arg) (3). Increased NO production enhances endothelial function, which is lost during aging. WT-BPIFB4, which is less phosphorylated, show less 14-3-3 affinity, is more nuclear (4), and is therefore less efficient in activating eNOS as compared with LAV-BPIFB4.

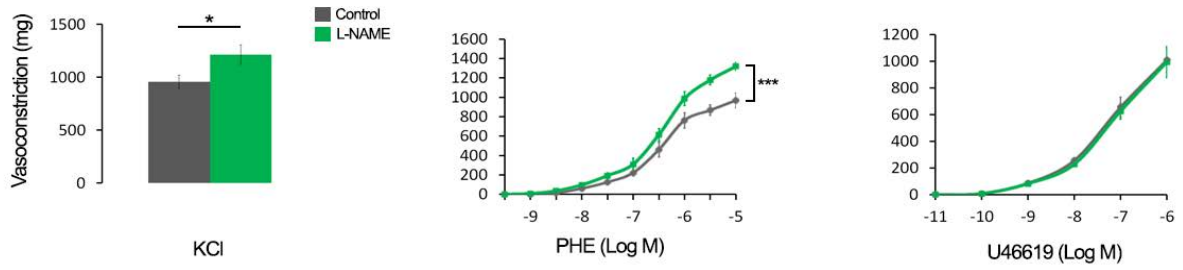

Online Figure XIV. Effect of L-NAME on potassium, phenylephrine and U46619 vasoconstriction in mice mesenteric arteries.

Graphs show, from left to right, the vascular response of *ex vivo* mouse mesenteric arteries to potassium (80mM KCl), and the dose–responses to phenylephrine (PE), and thromboxane agonist U46619. The vascular responses are measured before (◆) and after L-NAME (300µM) exposure (■). Values are means±SEM. N=5 experiments per group. Statistics was performed using ANOVA; **P*<0.05; ****P*<0.001, before vs. after L-NAME.

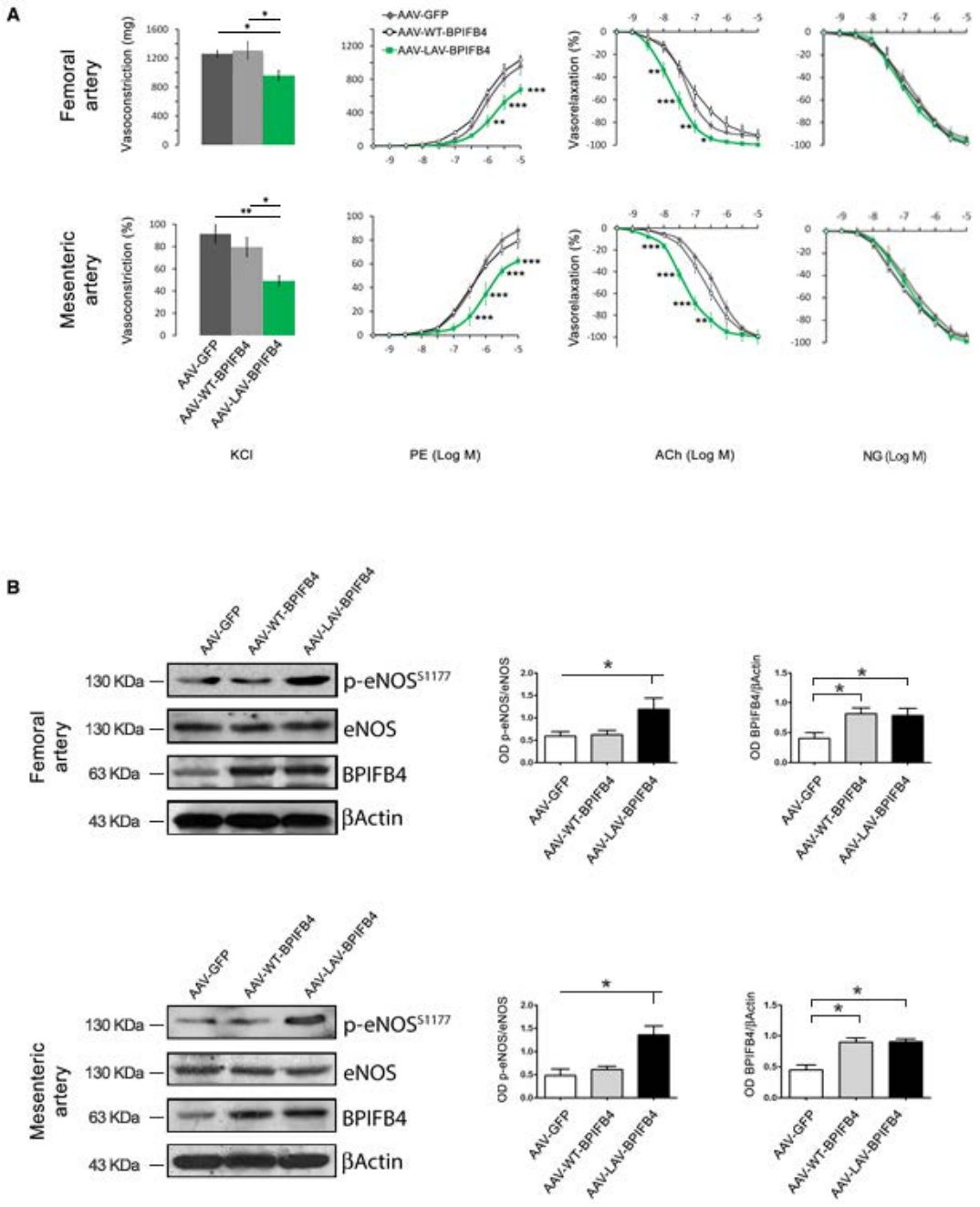

Online Figure XV. Expressional and vascular responses of vessels from mice infected with AAV-LAV-BPIFB4.

A, The graphs show, from the left to the right, the vascular response of femoral (first row) and mesenteric (second row) arteries to potassium (80mM KCl), and the dose–response to phenylephrine (PE), acetylcholine (ACh) and nitroglycerine. For these ex vivo studies, vessels were harvested from mice injected with AAV-GFP (◆), AAV-WT-BPIFB4 (○) or AAV-LAV-BPIFB4 (■). Values are means±SEM. N=4 experiments per group.*, $P<0.05$; **$P<0.01$; ***$P<0.001$ (ANOVA). **B,** Western blot of four pooled experiments on *ex vivo* femoral (first row) and mesenteric (second row) arteries from mice injected with AAV-GFP, AAV-WT-BPIFB4 or AAV-LAV-BPIFB4. Right graphs show quantification of eNOS

phosphorylation and BPIFB4. Values are means±SEM, N=2 pools of experiments. Statistic was performed using ANOVA; *P<0.05.

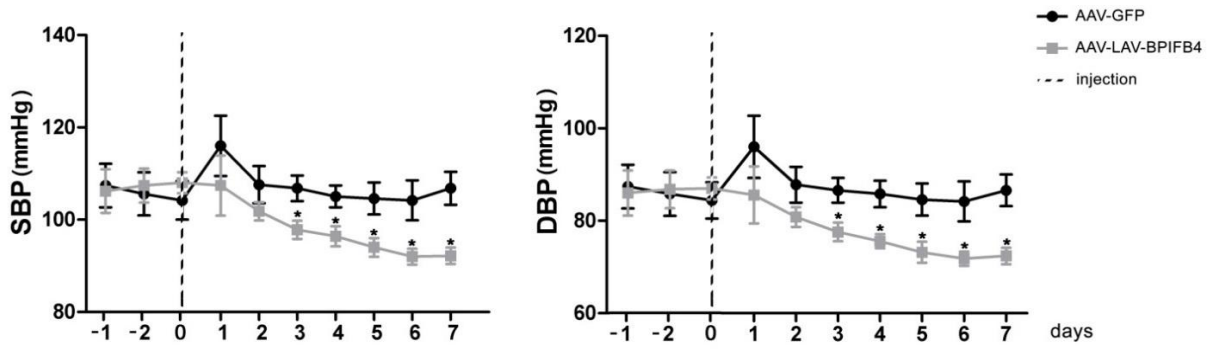

Online Figure XVI. Effect of AAV-LAV-BPIFB4 on blood pressure levels in normotensive mice.
Systolic (SBP, on the left) and diastolic blood pressure (DBP, on the right) in C57BL/6 mice treated with AAV-GFP (●) or AAV-LAV-BPIFB4 (■) (N=5/group). Measurements conducted before injection (reported on the x axis) were considered as basal values. Data are given as mean±SEM. *P<0.05 vs. AAV-GFP (unpaired t-test).

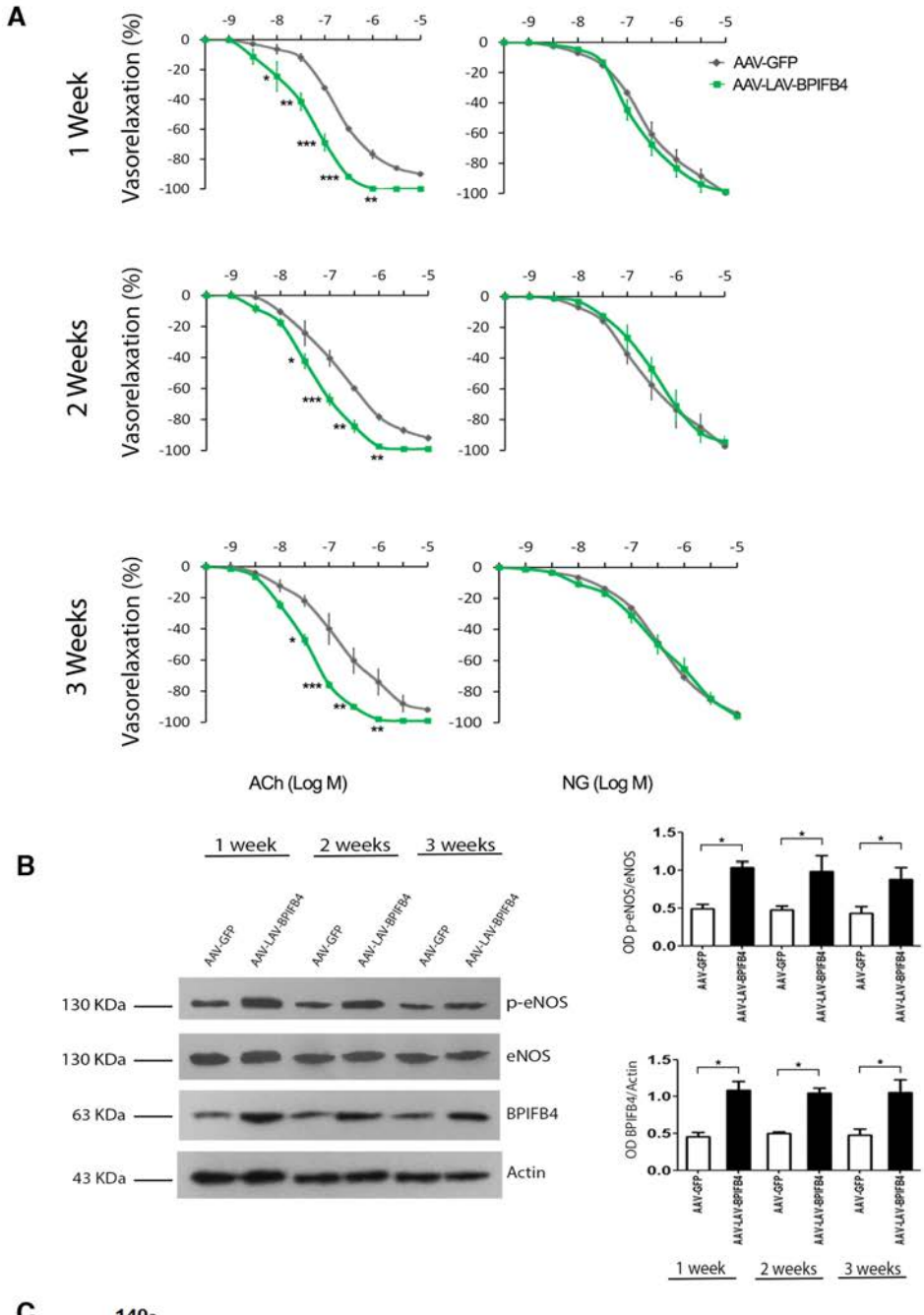
A
1 Week
2 Weeks
3 Weeks
Vasorelaxation (%)
AAV-GFP
AAV-LAV-BPIFB4
ACh (Log M)
NG (Log M)
B
1 week
2 weeks
3 weeks
AAV-GFP
AAV-LAV-BPIFB4
130 KDa
p-eNOS
eNOS
63 KDa
BPIFB4
43 KDa
Actin
OD p-eNOS/eNOS
OD BPIFB4/Actin
C
SBP (mmHg)
injection
days

Online Figure XVII. Durability of transgene expression and vascular responses following AAV-LAV-BPIFB4 delivery in normotensive mice.

A, Graphs show the dose-response curves of *ex vivo* mesenteric arteries, from mice injected with AAV-GFP(◆) or AAV-LAV-BPIFB4(■), to acetylcholine (ACh) and nitroglycerin (NG). Experiments were performed at 1 (first row), 2 (second row) and 3 weeks (third row) after gene delivery. Values are means±SEM. N=5 experiments per group. Statistics was performed using ANOVA; **P*<0.05; ***P*<0.01; ****P*<0.001. **B,** Representative Western blot for eNOS phosphorylation and BPIFB4 levels in mesenteric arteries of mice injected with AAV-GFP or AAV-LAV-BPIFB4. The right graph gives the quantification of eNOS phosphorylation and BPIFB4 level of three independent experiments. **C,** Systolic blood pressure (SBP) in mice treated with AAV-GFP (● ; *n*=5) or AAV-LAV-BPIFB4 (● ; *n*=5). Values are means±SEM. Statistics was performed using ANOVA; **P*<0.05; ***P*<0.01; ****P*<0.001.

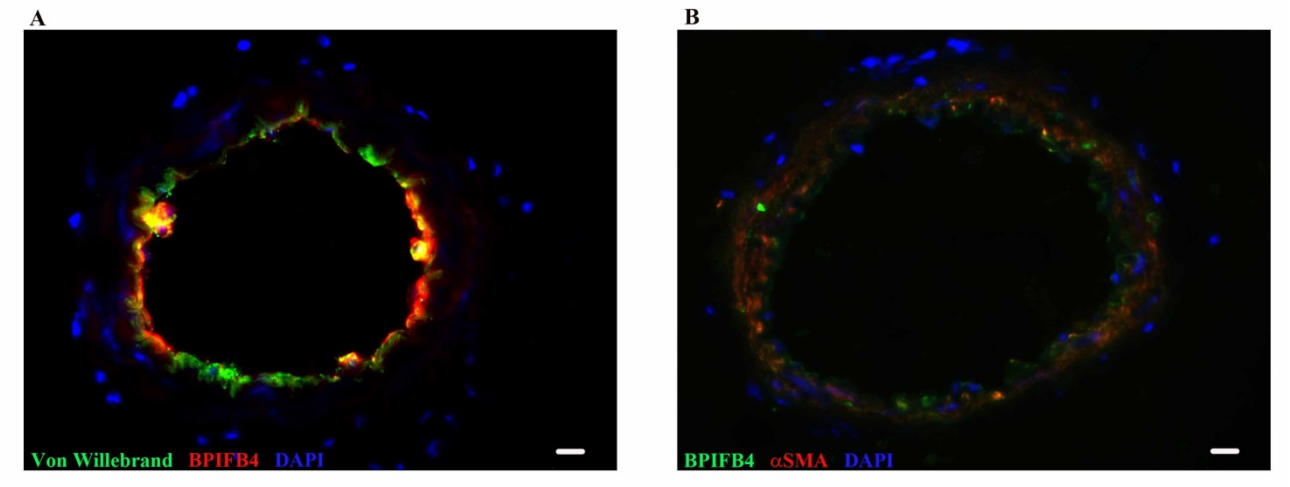

Online Figure XVIII. Immunostaining analysis of BPIFB4 in mesenteric artery of mice infected with AAV-LAV-BPIFB4.
The BPIFB4 signal co-localizes (yellow signal) with Von Willebrand signal in endothelial cells (A) and with α-SMA signal in smooth muscle vessel wall (B). Bar= 100um.

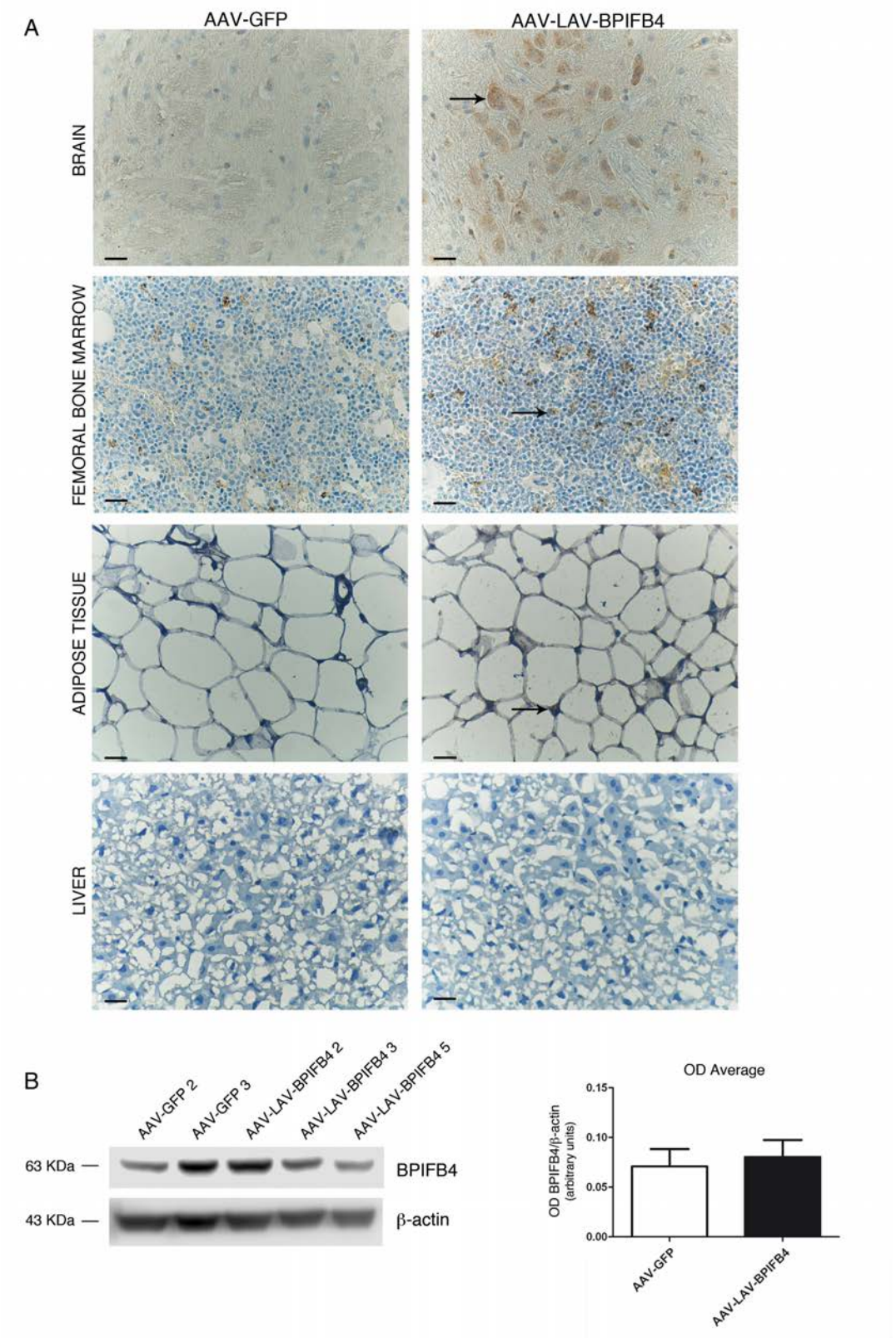

Online Figure XIX. BPIFB4 expression in tissues of infected mice and MNCs from infected rats.
A, Immunohistochemical analysis of BPIFB4 in different tissues of mice infected with AAV-GFP or AAV-LAV-BPIFB4. BPIFB4 overexpression (brown signals indicated by arrows) was detected in brain, femoral bone marrow and adipose tissue, but not in the liver of mice injected with AAV-LAV-BPIFB4. Bar = 40μm. **B,** Representative Western blot of BPIFB4 expression in MNCs of rats injected with AAV-

GFP (N=2) or AAV-LAV-BPIFB4 (N=3) on the left. The right graph gives the average quantification of BPIFB4 vs. β-actin. No significant difference between two groups was detected (unpaired t-test). Values are means±SEM.

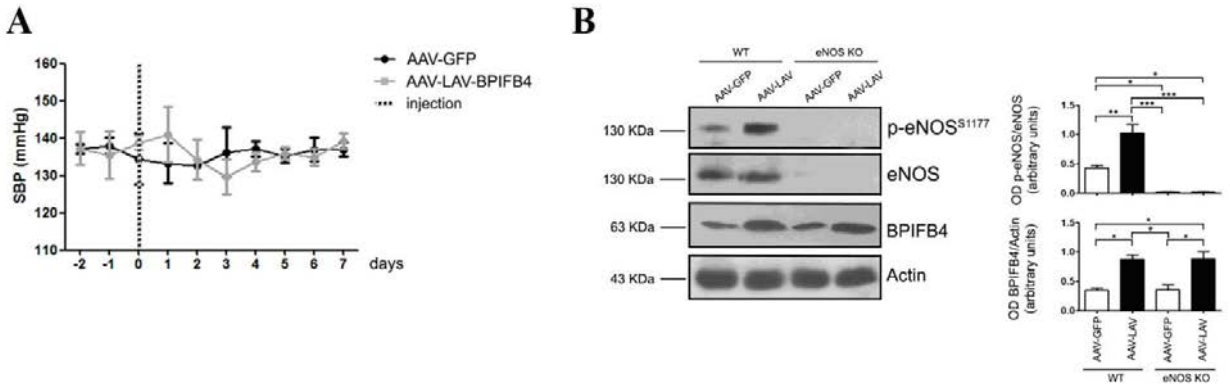

Online Figure XX. Effects of AAV-LAV-BPIFB4 in eNOS knockout mice.
A, Systolic blood pressure (SBP)in eNOS knockout mice treated with AAV-GFP (● ; *n*=5) or AAV-LAV-BPIFB4 (■ ; *n*=5).Values are means±SEM. **B**, Representative Western blot for eNOS phosphorylation and BPIFB4 levels in mesenteric arteries of eNOS knockout mice injected with AAV-GFP or AAV-LAV-BPIFB4. The right graph gives the quantification of eNOS phosphorylation and BPIFB4 levels of three experiments. Statistics was performed using ANOVA; **P*<0.05; ***P*<0.01; ****P*<0.001.

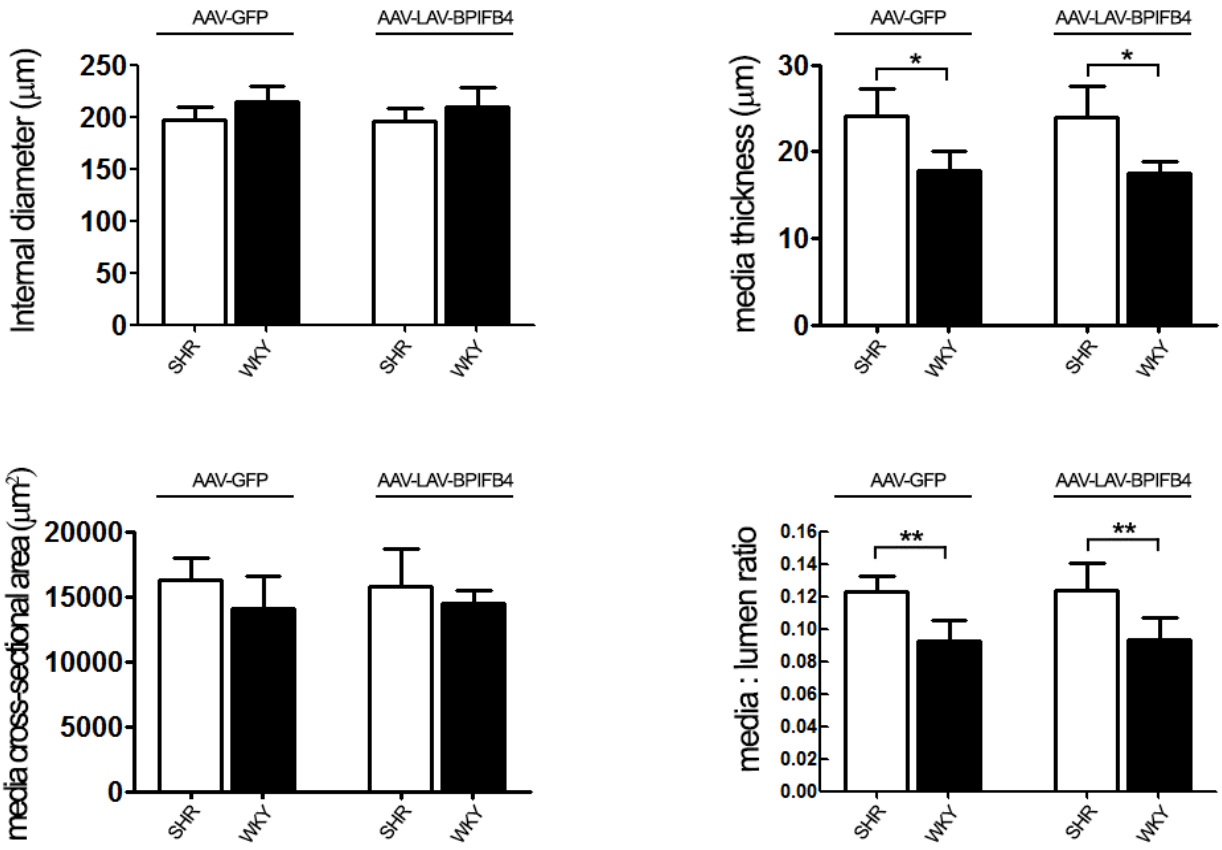

Online Figure XXI. Vascular remodeling in SHR and Wistar rats injected with AAV-LAV-BPIFB4. Bar graphs demonstrate morphological characteristics of small mesenteric arteries in SHRs (N=5) and their normotensive controls (WKY rats; N=5) injected with AAV-GFP or AAV-LAV-BPIFB4. Statistics was performed using ANOVA; **P*<0.05, ***P*< 0.01.

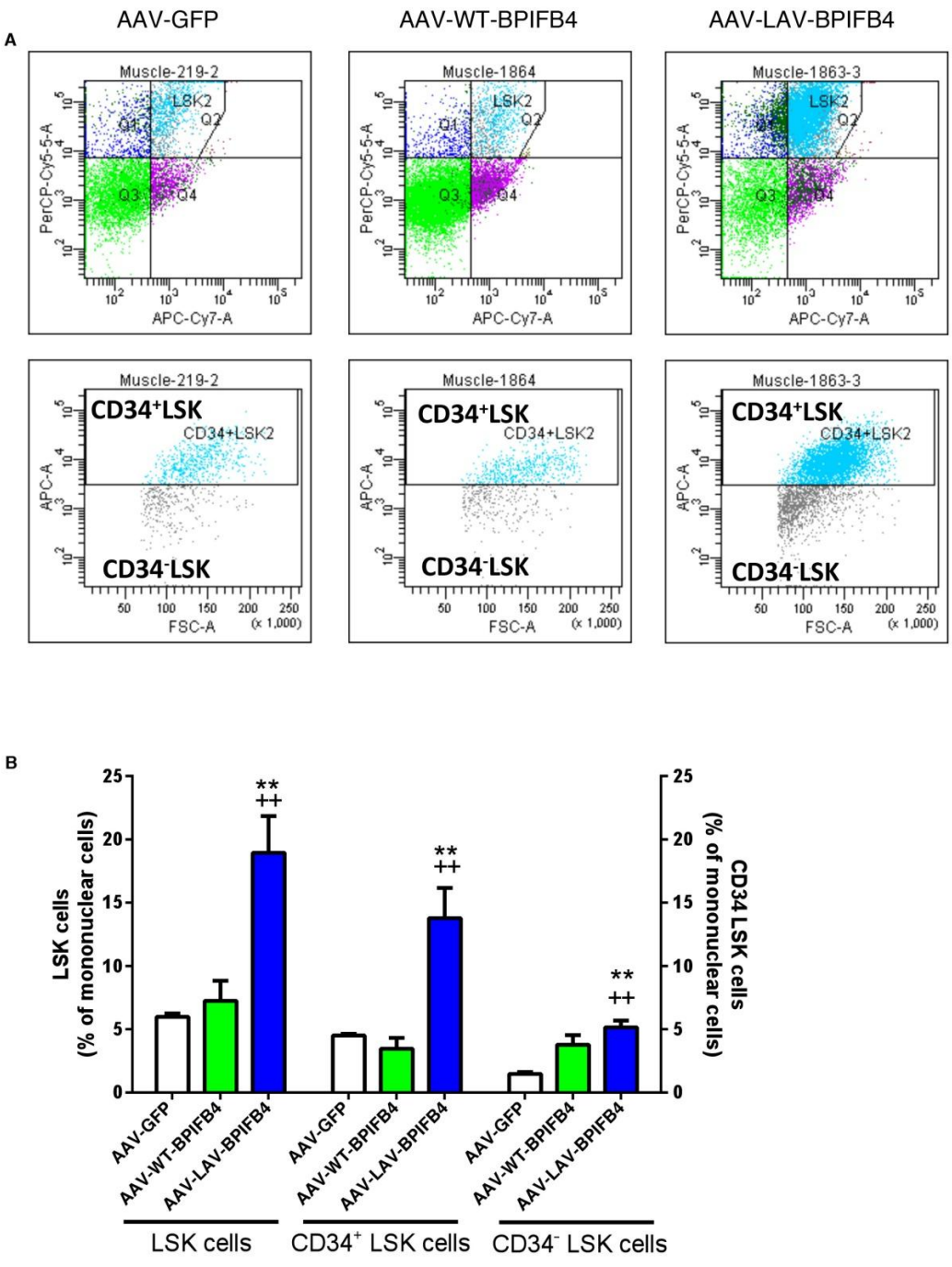

Online Figure XXII. Homing of stem cells to ischemic muscles.
Mice were infected systemically with AAV-WT-BPIFB4, AAV-LAV-BPIFB4 or received vehicle (AAV-GFP) through the tail vein before induction of femoral artery occlusion. Samples were collected 3 days post-ischemia. **A,** representative gating strategy for LSK and CD34/ LSK fractions. **B,** bar graphs showing average values in ischemic muscles. Data are mean (SE). $^{**}P<0.01$ vs vehicle, $^{++}P<0.01$ vs WT.

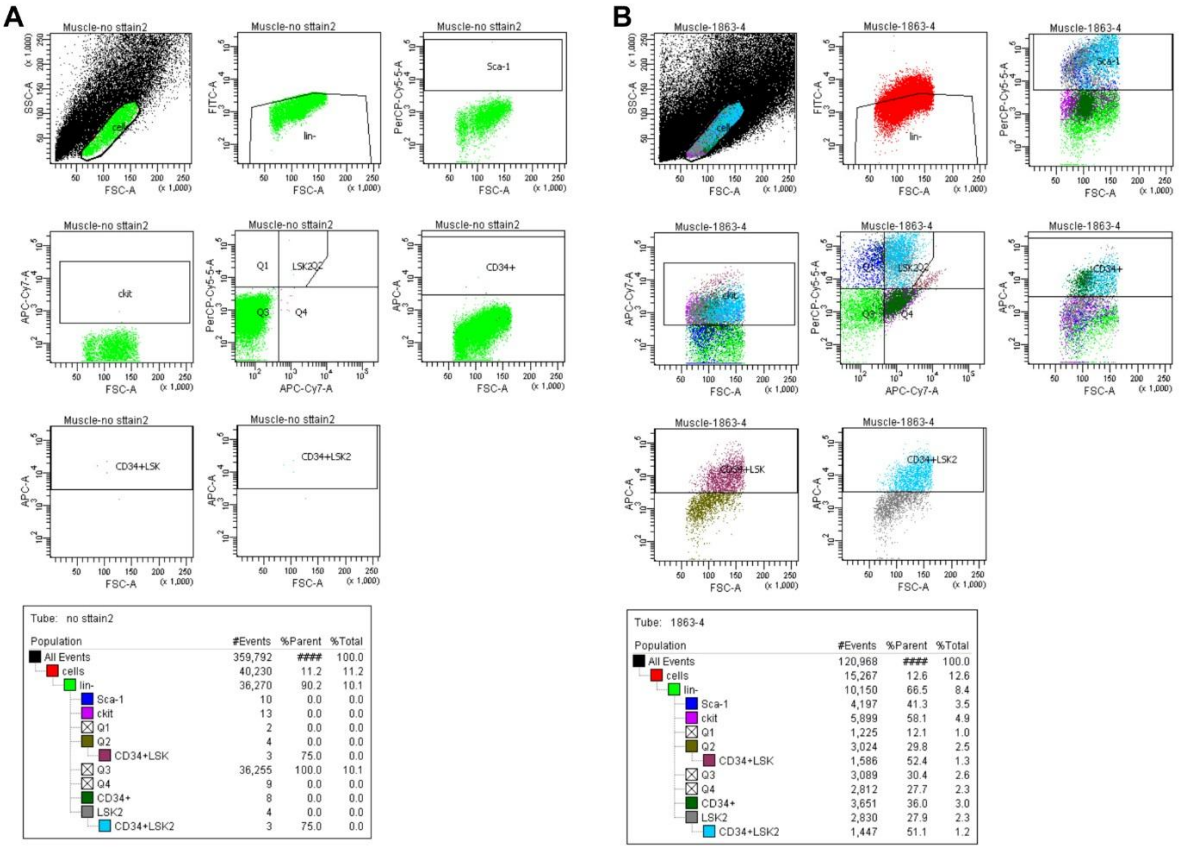

Tube: no sttain2			
Population	#Events	%Parent	%Total
All Events	359,792	####	100.0
cells	40,230	11.2	11.2
lin-	36,270	90.2	10.1
Sca-1	10	0.0	0.0
ckit	13	0.0	0.0
Q1	2	0.0	0.0
Q2	4	0.0	0.0
CD34+LSK	3	75.0	0.0
Q3	36,255	100.0	10.1
Q4	9	0.0	0.0
CD34+	8	0.0	0.0
LSK2	4	0.0	0.0
CD34+LSK2	3	75.0	0.0

Tube: 1863-4			
Population	#Events	%Parent	%Total
All Events	120,968	####	100.0
cells	15,267	12.6	12.6
lin-	10,150	66.5	8.4
Sca-1	4,197	41.3	3.5
ckit	5,899	58.1	4.9
Q1	1,225	12.1	1.0
Q2	3,024	29.8	2.5
CD34+LSK	1,586	52.4	1.3
Q3	3,089	30.4	2.6
Q4	2,812	27.7	2.3
CD34+	3,651	36.0	3.0
LSK2	2,830	27.9	2.3
CD34+LSK2	1,447	51.1	1.2

Online Figure XXIII. Gating strategy of LSK cells.
A, Gating of control samples in which the antibody was omitted. **B,** gating of samples showing initial identification of cells followed by definition of lineage negative elements and then definition of Sca-1 and cKit populations. Among the LSK cells, the two sub-fractions of CD34 positive and negative progenitor cells were finally distinguished.

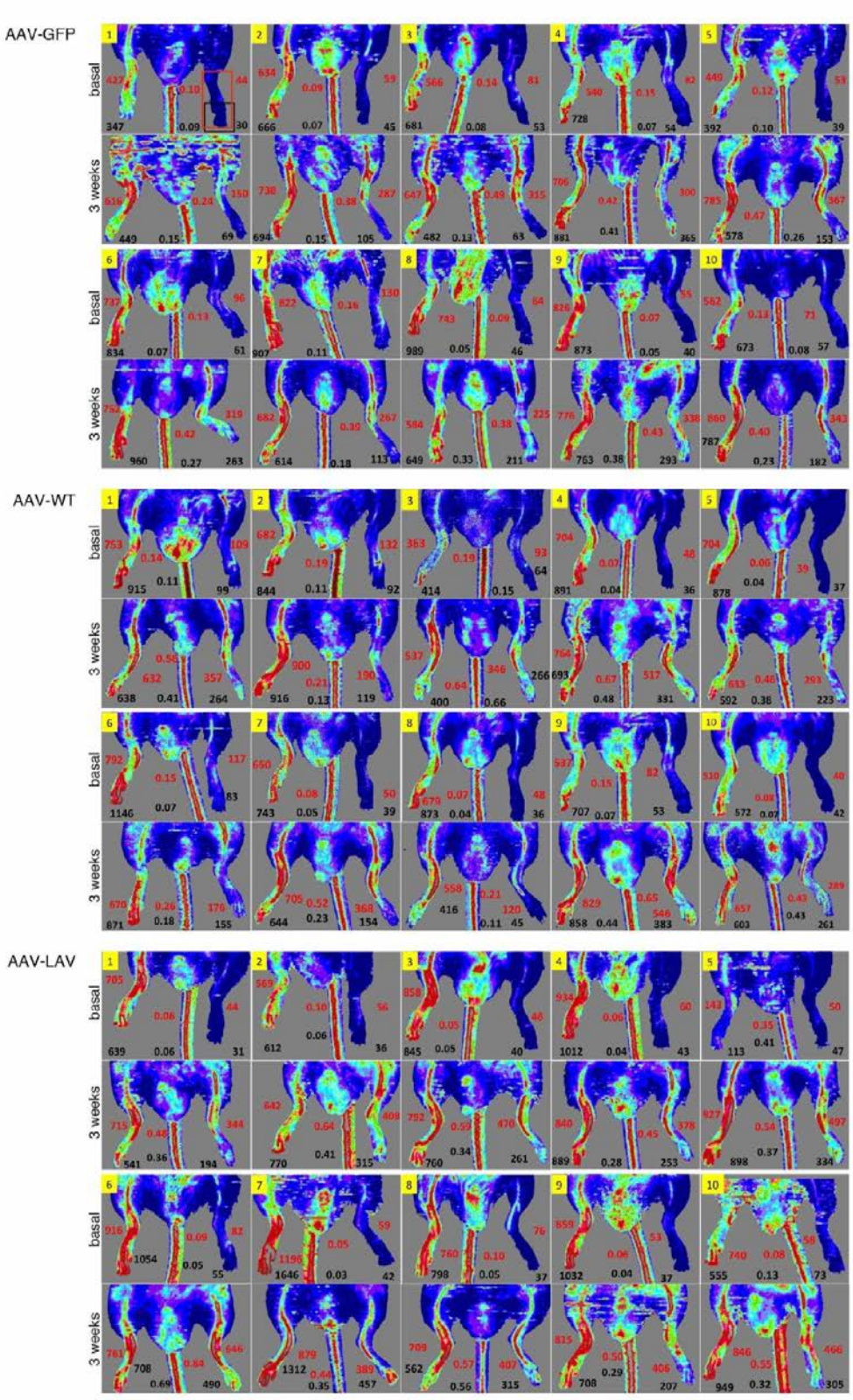

Online Figure XXIV. Effect of LAV-BPIFB4 on post-ischemic recovery of superficial blood flow.
Images of laser Doppler flowmetry captured at 0 and 21 days after induction of limb ischemia. Values represent arbitrary blood flow units taken at the level of the foot (black font) and whole limb (red font). The ratio of ischemic to contralateral side is also shown between each side values. N=10 in each group.

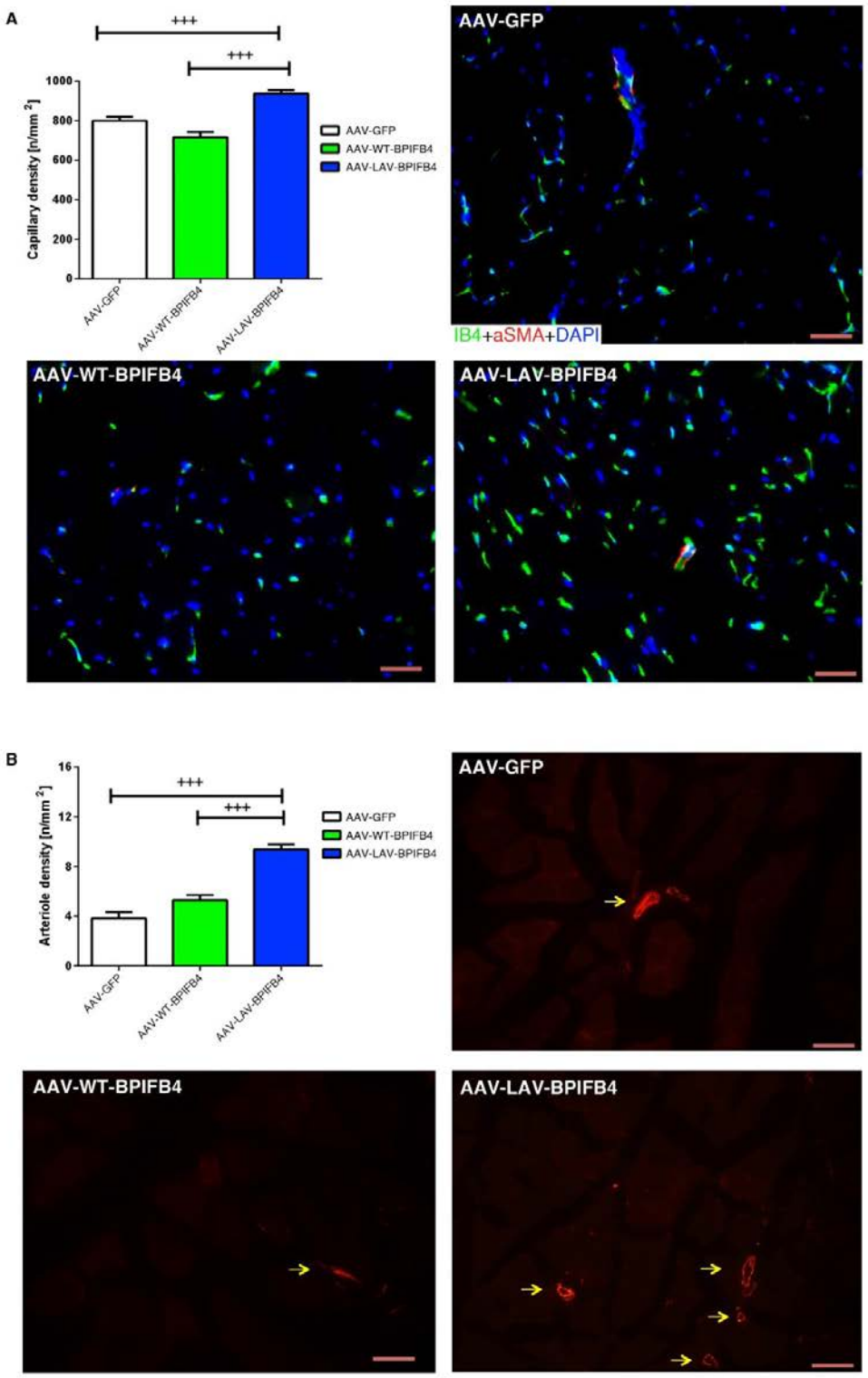

Online Figure XXV. Revascularization effect of LAV-BPIFB4 in mouse model of hindlimb ischemia. **A**, capillary density and **B**, arteriole density, as assessed 3 weeks post-ischemia. Values are mean±SEM of N=7–10 in each group. Bar = 50 μm.

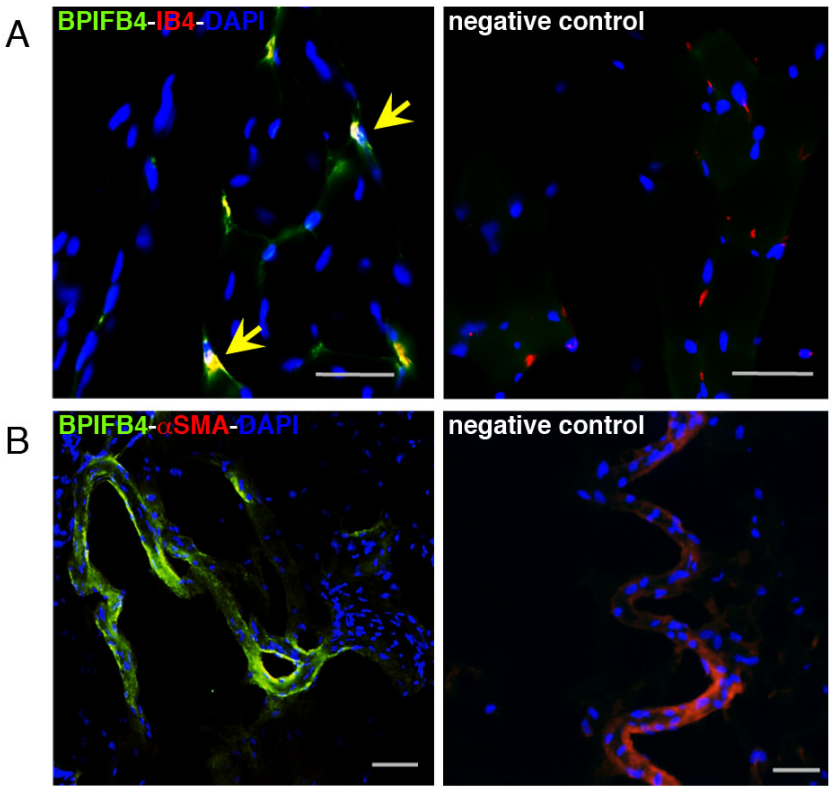

Online Figure XXVI. Immunofluorescence microscopy images showing transgene expression at 3 weeks after AAV-LAV-BPIFB4 intravenous injection and induction of limb ischemia. Ischemic adductor muscle sections were stained with anti-BPIFB4, IB4/a-SMA and DAPI. **A**, IB4 positive capillary endothelial cells and **B**, alpha-SMA positive arterioles from muscles of mice injected with AAV-LAV-BPIFB4 express abundantly the transgene. Yellow arrows indicate co-localization between BPIFB4 and IB4 signals. Bar=50um.

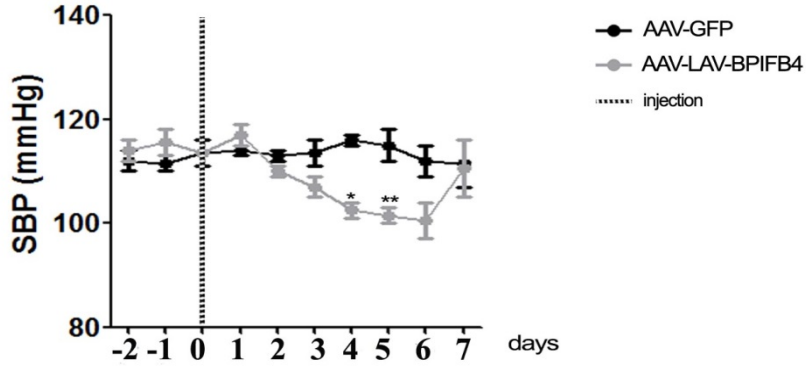

Online Figure XXVII. Effect of AAV-LAV-BPIFB4 on mice systolic blood pressure after vein injection. Systolic blood pressure (SBP) in mice treated with AAV-GFP (● ; *n*=5) or AAV-LAV-BPIFB4 (● ; *n*=5). Values are means ± SEM. Statistics was performed using ANOVA; *, $p<0.05$; **, $p<0.01$.

ONLINE TABLES

Online Table I. Association Tests Results in the Screening Set and Replication Cohorts.

SNP	Assoc. Model	Cohort	a/A	MAF	Allele or Genotype	No. (%) of Alleles/Genotypes		*P*-value	OR (95%CI)
						LLIs	Controls		
rs7583529	RM	SICS-scr	A/G	0.21	AA	37 (9)	17 (3)	$6.45x10^{-5}$	3.15 (1.75–5.68)
		GLS-rep	A/G	0.22	AA	83 (5)	53 (5)	0.69	1.07 (0.75–1.53)
		USA-rep	-- Not tested --						
rs571391	DM	SICS-scr	G/A	0.43	GG/GA	241 (59)	399 (72)	$1.39x10^{-5}$	0.55 (0.42–0.72)
		GLS-rep	G/A	0.34	GG/GA	903 (57)	623 (57)	0.93	0.99 (0.85–1.16)
		USA-rep	-- Not tested --						
rs285097	AM	SICS-scr	G/T	0.08	G	43 (5)	116 (10)	$3.79x10^{-5}$	0.47 (0.33–0.68)
		GLS-rep	G/T	0.07	G	195 (6)	150 (7)	0.26	0.88 (0.71–1.10)
		USA-rep	-- Not tested --						
rs2070325	RM	SICS-scr	G/A	0.30	GG	57 (14)	35 (6)	$5.98x10^{-5}$	2.42 (1.56–3.77)
		GLS-rep	G/A	0.36	GG	225 (14)	112 (10)	0.0036	1.43 (1.12–1.80)
		USA-rep	G/A	0.35	GG	196 (13)	46 (9)	0.0063	1.60 (1.14–2.24)

SNP, dbSNP ID; Assoc. Model, associated genetic model (AM = allelic model, DM = dominant model, RM = recessive model); Cohort, analysed cohort (SICS-scr = Southern Italian Centenarian Study screening cohort, GLS-rep = German Longevity Study replication cohort, USA-rep = United States-American replication cohort); a/A, minor allele/major allele based on whole sample; MAF, minor allele frequency; No. (%) Alleles/Genotypes, number and percentage of reference alleles/genotypes in long-living individuals (LLIs) and control individuals (controls); OR, odds ratio; 95% CI, 95% confidence interval.

Online Table II. Genotype counts.

Cohort	CHR	SNP	m	M	LLIs	CTRLs
SICS-scr	20	rs2070325	G	A	57/146/201	35/250/266
GLS-rep	20	rs2070325	G	A	225/715/659	112/545/432
USA-rep	20	rs2070325	G	A	196/648/617	46/242/232

Cohort, analysed cohort; Chr, Chromosome; m, minor allele; M, major allele; LLIs, number of mm/mM/MM genotypes in cases; CTRLs, number of mm/mM/MM genotypes in controls SICS-scr, Italian screening set; GLS-rep, German replication set; USA-rep, American replication set.

Online Table III. Comparison of HEK293T cell transcriptional profiles after transfection with WT-BPIFB4 or empty vector

Gene	WT.AVG_Signal	Empty.AVG_Signal	FC	*P*-value	Regulation	Exosome
HSPA6	11384.717	625.217	4.187	<0.001	Up	no
HSPA7	3907.633	288.367	3.76	<0.001	Up	no
LOC652750	1699	144.433	3.556	<0.001	Up	no
TCEAL7	962.833	129.1	2.899	<0.001	Up	no
HSPA1A	559.4	136.1	2.039	<0.001	Up	no
DNAJB1	5896.7	1485.233	1.989	<0.001	Up	no
HS.543887	1011.633	333.2	1.602	<0.001	Up	no
RNU1-3	970	353.033	1.458	<0.001	Up	yes
ZFAND2A	1495.133	570.9	1.389	<0.001	Up	no
RNU1-5	1162.2	452.267	1.362	<0.001	Up	yes
PPIL2	378.7	148.967	1.346	<0.001	Up	no
RNU1G2	824.4	338.467	1.284	<0.001	Up	yes
HS.579631	20786.367	8670.467	1.261	<0.001	Up	no
MIR1974	589.2	248.567	1.245	<0.001	Up	yes
SCARNA8	1005.6	424.967	1.243	<0.001	Up	no
RN5S9	1421.2	610.4	1.219	<0.001	Up	yes
BAG3	3604.067	1551.067	1.216	<0.001	Up	no
MUM1	512.2	226.133	1.18	<0.001	Up	no
HSPA1B	22851.5	10136.333	1.173	<0.001	Up	no
SNORD83B	798.133	356.433	1.163	<0.001	Up	no
RNU4ATAC	382.867	172.033	1.154	<0.001	Up	no
PPP1R15A	1626.667	732.833	1.15	<0.001	Up	no
SNORA79	1026.833	468.367	1.132	<0.001	Up	no
SNORD15B	404.033	185.933	1.12	<0.001	Up	no
RNU1F1	631	291.533	1.114	<0.001	Up	yes
RNU1A3	1156.467	541.533	1.095	<0.001	Up	yes
HSPB1	3392.8	1656	1.035	<0.001	Up	yes
SCARNA14	466.6	231.567	1.011	<0.001	Up	no
BCYRN1	3007.433	1501.1	1.003	<0.001	Up	yes
LOC388796	2132.833	1071.933	0.993	<0.001	Up	no
NBPF20	1448.6	2974.55	-1.038	<0.001	Down	yes
LOC440092	144.1	308.9	-1.1	<0.001	Down	no
SNORA71C	681.2	1534.4	-1.172	<0.001	Down	no

WT.AVG_Signal: average of fluorescence signals of HEK293T transfected with vector encoding for WT-BPIFB4 (n=3); Empty. AVG_Signal: average of fluorescence signals of HEK293T transfected with empty vector (n=3); FC: fold change; Exosome: RNA detected by de Jong et al.[28] in exosomes produced by endothelial cells under stress conditions. Only genes with *P*-value < 0.001 are indicated.

Online Table IV. Comparison of HEK293T cell transcriptional profiles after transfection with LAV-BPIFB4 or empty vector

Gene	LAV.AVG_Signal	Empty.AVG_Signal	FC	*P*-value	Regulation	Exosome
HSPA7	5512.1	288.367	4.257	<0.001	Up	no
HSPA6	10394	625.217	4.055	<0.001	Up	no
LOC652750	1522.833	144.433	3.398	<0.001	Up	no
TCEAL7	892.933	129.1	2.79	<0.001	Up	no
HSPA1A	835.167	136.1	2.617	<0.001	Up	no
HS.543887	1532.6	333.2	2.202	<0.001	Up	no
MIR1974	1029.433	248.567	2.05	<0.001	Up	yes
DNAJB1	6058.167	1485.233	2.028	<0.001	Up	no
RN5S9	2194.433	610.4	1.846	<0.001	Up	yes
SCARNA8	1439.133	424.967	1.76	<0.001	Up	no
SNORD15B	606.1	185.933	1.705	<0.001	Up	no
RNU1G2	1070	338.467	1.661	<0.001	Up	yes
RNU1-3	1113.7	353.033	1.657	<0.001	Up	yes
ZFAND2A	1769.933	570.9	1.632	<0.001	Up	no
RNU1-5	1373.3	452.267	1.602	<0.001	Up	yes
PPIL2	443.183	148.967	1.573	<0.001	Up	no
SCARNA14	685.433	231.567	1.566	<0.001	Up	no
SNORA79	1362.733	468.367	1.541	<0.001	Up	no
RNU4ATAC	493.167	172.033	1.519	<0.001	Up	no
SNORD83B	995.333	356.433	1.482	<0.001	Up	no
LOC100130516	10136.8	3635.233	1.479	<0.001	Up	yes
SCARNA23	551.133	199.267	1.468	<0.001	Up	no
BCYRN1	4118.2	1501.1	1.456	<0.001	Up	yes
RNY1	607.7	236.333	1.363	<0.001	Up	yes
FLJ36131	5761.433	2291.833	1.33	<0.001	Up	yes
SNORA12	1746.067	700.133	1.318	<0.001	Up	no
CATSPER2	8787.5	3526.733	1.317	<0.001	Up	yes
RNU1A3	1348.133	541.533	1.316	<0.001	Up	yes
LOC648852	1625.567	654.567	1.312	<0.001	Up	yes
BAG3	3808.633	1551.067	1.296	<0.001	Up	no
SCARNA18	572.833	234.867	1.286	<0.001	Up	no
SNORD13	642.833	265.5	1.276	<0.001	Up	yes
RNU1F1	693.633	291.533	1.251	<0.001	Up	yes
TRK1	503.633	218.433	1.205	<0.001	Up	no
SNORA42	409.9	182.067	1.171	<0.001	Up	no
PPP1R15A	1604.067	732.833	1.13	<0.001	Up	no
HS.579631	18840.5	8670.467	1.12	<0.001	Up	no
HS.129244	320.5	147.6	1.119	<0.001	Up	no
TRQ1	347.333	160.167	1.117	<0.001	Up	no
MIR1978	6763.4	3140	1.107	<0.001	Up	yes
HS.25892	4475.233	2083.5	1.103	<0.001	Up	no
LOC100132585	2751.167	1280.533	1.103	<0.001	Up	yes
SNORA27	386.5	180.8	1.096	<0.001	Up	no
LOC388796	2274.2	1071.933	1.085	<0.001	Up	no
RNU86	643.767	303.767	1.084	<0.001	Up	no
SCARNA13	2019.2	957.4	1.077	<0.001	Up	no
SCARNA16	661.833	313.933	1.076	<0.001	Up	no
E2F2	1587.733	757.467	1.068	<0.001	Up	no
SNORD4A	812.967	390.567	1.058	<0.001	Up	no

HS.163752	1896.833	932.633	1.024	<0.001	Up	no
SNORD3D	801.6	399.067	1.006	<0.001	Up	yes
SNORD38A	474.133	237.1	1	<0.001	Up	no
DYNLT3	352.9	709.067	-1.007	<0.001	Down	no
TULP4	152.733	308.883	-1.016	<0.001	Down	no
NBPF20	1442.15	2974.55	-1.044	<0.001	Down	yes
SNORA71C	700.167	1534.4	-1.132	<0.001	Down	no
LOC440092	136.8	308.9	-1.175	<0.001	Down	no

LAV.AVG Signal: average of fluorescence signals of HEK293T transfected with vector encoding for LAV-BPIFB4 (n=3); Empty. AVG Signal: average of fluorescence signals of HEK293T transfected with empty vector (n=3); FC: fold change; Exosome: RNA detected by de Jong et al.[28] in exosomes produced by endothelial cells under stress conditions. Only genes with *P*-value < 0.001 are indicated in the table.

Online Table V. Comparison of HEK293T cell transcriptional profiles after transfection with LAV-BPIFB4 or WT-BPIFB4

Gene	LAV.AVG_Signal	WT.AVG_Signal	FC	*P*-value	Regulation	Exosome
LOC648852	1625.567	793.333	1.035	<0.001	Up	yes
MIR1974	1029.433	589.2	0.805	<0.001	Up	yes
LOC100132673	8167.1	4837.867	0.755	<0.001	Up	yes
HS.163752	1896.833	1141.267	0.733	<0.001	Up	no
LOC100131713	6172.983	10548.7	-0.773	<0.001	Down	yes

LAV.AVG Signal: average of fluorescence signals of HEK293T transfected with vector encoding for LAV-BPIFB4 (n=3); WTAVG Signal: average of fluorescence signals of HEK293T transfected with vector encoding for WT-BPIFB4 (n=3); FC: fold change; Exosome: RNA detected by de Jong et al.[28] in exosomes produced by endothelial cells under stress conditions. Only genes with *P*-value < 0.001 are indicated in the table.

Online Table VI. *P*-values generated by the comparison of the transcriptional profiles for ribosomal, translational, and exosomal categories.

Comparison	Total # genes	Ribosome		Translation		Exosome	
		# genes	*P*-value	# genes	*P-value*	# genes	*P*-value
WT_Empty	1558	72	2.00E-14	77	4.83E-07	462	<1.00E-11
LAV_Empty	2291	85	2.87E-09	78	0.02	621	<1.00E-11
LAV_WT	816	32	7.50E-05	37	0.001	300	<1.00E-11

Total # genes: total number of modulated genes for the respective comparison; # genes: number of modulated genes for the respective comparison in the indicated category.

Online Table VII. GO categories for ribosome and translation

ribosome	
ribosomal small subunit biogenesis	biological_process
organellar large ribosomal subunit	cellular_component
organellar ribosome	cellular_component
cytosolic ribosome	cellular_component
large ribosomal subunit	cellular_component
structural constituent of ribosome	molecular_function
mature ribosome assembly	biological_process
ribosome biogenesis	biological_process
mitochondrial ribosome	cellular_component
ribosome	cellular_component
cytosolic small ribosomal subunit	cellular_component
small ribosomal subunit	cellular_component
cytosolic large ribosomal subunit	cellular_component
mitochondrial large ribosomal subunit	cellular_component
ribosomal subunit	cellular_component
organellar small ribosomal subunit	cellular_component
mitochondrial small ribosomal subunit	cellular_component
ribosomal large subunit biogenesis	biological_process
translation	
translational elongation	biological_process
translation	biological_process
translational initiation	biological_process
cotranslational protein targeting to membrane	biological_process
translational termination	biological_process
SRP-dependent cotranslational protein targeting to membrane	biological_process

Online Table VIII. Capillary density values

Vehicle											
section	**cage number (sequence mouse number)**										
	E1 (1)	**E2 (2)**	**E3 (3)**	**E4 (4)**	**E5 (5)**	**I3 (8)**	**I5 (10)**				
1	933.927	417.526	629.501	940.498	1253.421	784.378	1189.772				
2	534.76	492.348	725.97	491.27	990.123	904.101	893.83				
3	847.806	492.248	424.717	1014.139	1284.985	297.734	356.245				
4	858.771	745.385	467.191	432.308	1178.67	976.358	895.904				
5	733.411	674.779	785.207	131.423	1015.569	1061.318	1422.481				
6	589.335	374.643	699.76	533.982	855.53	1516.8	979.191				
7	252.7	735.34	600.003	918.48	1061.758	829.71	1092.182				
8	263.139	394.141	751.368	409.022	908.463	1197.117	1782.812				
9	204.725	457.735	827.846	840.393	853.476	1429.76	1543.926				
10	272.293	703.798	639.359	1526.879	721.679	979.313	933.409	**Mean**			
Means	549.087	548.794	655.092	723.839	1012.367	997.659	1108.975	**799.402**			

WT											
section	**cage number (sequence mouse number)**										
	G1 (1)	**G2 (2)**	**G3 (3)**	**G4 (4)**	**G5 (5)**	**K1 (6)**	**K2 (7)**	**K3 (8)**	**K4 (9)**	**K5 (10)**	
1	1075.372	778.469	633.559	1350.421	353.931	1277.027	920.691	368.298	399.242	645.129	
2	720.259	780.805	1177.509	711.703	722.327	552.915	753.504	749.555	515.065	666.64	
3	537.545	1227.233	506.912	782.636	606.483	560.957	642.205	350.027	220.406	80.861	
4	1286.197	1166.881	537.01	902.349	868.445	443.815	165.807	249.114	217.04	229.63	
5	1066.642	1156.438	1018.822	784.955	752.892	486.189	744.027	267.334	522.417	243.26	
6	1397.316	757.3	924.569	1212.149	559.027	556.119	976.956	290.216	565.096	420.109	
7	1095.653	770.232	1090.49	780.961	541.665	323.417	745.826	721.242	547.289	500.105	
8	905.076	675.261	845.47	697.009	933.395	760.706	479.028	404.003	595.461	546.625	
9	988.7	585.762	587.485	664.291	1082.285	1074.752	1001.76	1033.55	610.825	671.359	
10	772.944	775.836	951.611	706.367	741.237	1066.436	989.688	858.085	505.245	527.463	**Mean**
Means	984.570	867.422	827.344	859.284	716.169	710.233	741.95	529.143	469.809	453.118	**715.904**

LAV											
section	**cage number (sequence mouse number)**										
	F1 (1)	**F2 (2)**	**F5 (5)**	**J1 (6)**	**J2 (7)**	**J3 (8)**	**J5 (10)**				
1	417.329	1496.725	812.613	927.834	926.475	1048.525	904.747				
2	518.349	1023.32	957.99	474.512	813.301	1051.325	988.506				
3	589.384	1428.239	995.801	771.618	564.556	854.102	1271.395				
4	443.706	1150.827	780.886	1062.171	882.959	1046.717	959.946				
5	806.646	1268.649	715.626	1105.729	737.713	826.769	865.552				
6	1227.058	1132.843	826.744	775.295	803.885	591.252	1132.997				
7	1206.071	901.684	1015.68	1018.394	1251.181	758.848	1186.716				
8	867.688	932.133	1085.473	968.39	1044.566	423.642	1026.097				
9	699.105	1138.702	823.984	1279.175	718.023	956.728	1055.469				
10	970.825	1356.429	675.182	1228.665	650.524	1253.381	1038.567	**Mean**			
Means	774.616	1182.955	868.998	961.178	839.318	881.129	1042.999	**935.885**			

Online Table IX. Arteriole density values

Vehicle											
section	**cage number (sequence mouse number)**										
	E1 (1)	**E2 (2)**	**E3 (3)**	**E4 (4)**	**E5 (5)**	**I3 (8)**	**I5 (10)**				
1	9.019	4.45	11.66	4.071	1.95	4.765	15.19				
2	2.962	6.047	1.667	4.476	4.237	8.408	4.488				
3	0	0	3.136	5.161	6.258	5.607	1.427				
4	0	8.021	1.795	8.307	0	3.57	0				
5	3.732	1.46	0	8.735	4.396	3.387	4.185				
6	3.363	4.15	1.401	0	0	0	0				
7	1.762	8.027	2.789	0	0	1.594	5.609				
8	1.598	9.516	2.978	3.144	4.025	3.607	4.145				
9	1.482	6.014	6.406	0	0	6.567	0				
10	9.861	7.984	1.745	1.904	5.364	5.269	4.837	**Mean**			
Means	3.378	5.567	3.358	3.58	2.623	4.277	3.988	**3.824**			

WT											
section	**cage number (sequence mouse number)**										
	G1 (1)	**G2 (2)**	**G3 (3)**	**G4 (4)**	**G5 (5)**	**K1 (6)**	**K2 (7)**	**K3 (8)**	**K4 (9)**	**K5 (10)**	
1	3.045	0	4.709	2.734	5.924	4.624	4.523	5.335	1.474	17.356	
2	8.943	0	5.59	0	6.327	3.253	0	15.343	6.466	7.215	
3	8.932	1.65	9.28	0	2.687	2.934	0	14.382	2.964	16.612	
4	1.693	4.708	3.428	4.144	0	0	3.903	10.826	9.908	15.262	
5	0	0	5.379	5.039	4.573	8.175	6.609	13.606	0	13.998	
6	0	0	6.354	0	2.924	0	1.426	7.805	1.662	16.325	
7	3.438	1.747	2.933	0	4.567	0	0	6.625	7.691	13.454	
8	3.514	5.373	6.305	4.038	4.625	14.507	0	16.188	8.738	18.848	
9	1.79	7.879	5.186	8.568	7.72	7.427	1.886	7.345	8.584	2.974	
10	1.842	0	6.04	3.8	5.877	4.858	1.775	2.762	9.061	1.182	**Mean**
Means	3.32	2.136	5.521	2.832	4.522	4.578	2.012	10.022	5.655	12.321	**5.292**

LAV											
section	**cage number (sequence mouse number)**										
	F1 (1)	**F2 (2)**	**F5 (5)**	**J1 (6)**	**J2 (7)**	**J3 (8)**	**J5 (10)**				
1	0	16.222	8.408	3.926	13.774	18.986	8.379				
2	4.8	10.908	3.608	3.372	13.798	17.836	5.772				
3	0	11.916	7.325	1.651	14.563	6.918	3.069				
4	0	27.964	4.693	0	13.041	20.533	3.144				
5	2.284	25.598	9.725	6.883	6.615	21.306	1.369				
6	0	16.696	8.896	11.526	17.138	19.01	3.005				
7	3.521	11.54	7.019	3.519	5.566	23.049	3.99				
8	4.497	19.325	7.641	0	11.134	20.743	1.475				
9	6.751	21.024	8.254	6.691	13.355	6.056	6.76				
10	0	21.127	13.043	7.628	13.612	7.565	6.563	**Mean**			
Means	2.185	18.232	7.861	4.519	12.26	16.2	4.353	**9.373**			

SUPPLEMENTAL REFERENCES

1. Malovini A, Illario M, Iaccarino G, Villa F, Ferrario A, Roncarati R, Anselmi CV, Novelli V, Cipolletta E, Leggiero E, Orro A, Rusciano MR, Milanesi L, Maione AS, Condorelli G, Bellazzi R, Puca AA. Association study on long-living individuals from Southern Italy identifies rs10491334 in the CAMKIV gene that regulates survival proteins. *Rejuvenation Res.* 2011;14:283-291.

2. Nebel A, Kleindorp R, Caliebe A, Nothnagel M, Blanche H, Junge O, Wittig M, Ellinghaus D, Flachsbart F, Wichmann HE, Meitinger T, Nikolaus S, Franke A, Krawczak M, Lathrop M, Schreiber S. A genome-wide association study confirms APOE as the major gene influencing survival in long-lived individuals. *Mech Ageing Dev.* 2011;132:324-330.

3. Novelli V, Viviani Anselmi C, Roncarati R, Guffanti G, Malovini A, Piluso G, Puca AA. Lack of replication of genetic associations with human longevity. *Biogerontology.* 2008;9:85-92.

4. Geesaman BJ, Benson E, Brewster SJ, Kunkel LM, Blanche H, Thomas G, Perls TT, Daly MJ, Puca AA. Haplotype-based identification of a microsomal transfer protein marker associated with the human lifespan. *Proc Natl Acad Sci U S A.* 2003;100:14115-14120.

5. Spinetti G, Fortunato O, Caporali A, Shantikumar S, Marchetti M, Meloni M, Descamps B, Floris I, Sangalli E, Vono R, Faglia E, Specchia C, Pintus G, Madeddu P, Emanueli C. MicroRNA-15a and microRNA-16 impair human circulating proangiogenic cell functions and are increased in the proangiogenic cells and serum of patients with critical limb ischemia. *Circ Res.*112:335-346.

6. Spinetti G, Cordella D, Fortunato O, Sangalli E, Losa S, Gotti A, Carnelli F, Rosa F, Riboldi S, Sessa F, Avolio E, Beltrami AP, Emanueli C, Madeddu P. Global remodeling of the vascular stem cell niche in bone marrow of diabetic patients: implication of the microRNA-155/FOXO3a signaling pathway. *Circ Res.* 2013;112:510-522.

7. Bingle CD, Seal RL, Craven CJ. Systematic nomenclature for the PLUNC/PSP/BSP30/SMGB proteins as a subfamily of the BPI fold-containing superfamily. *Biochem Soc Trans.* 2011;39:977-983.

8. Andrault JB, Gaillard I, Giorgi D, Rouquier S. Expansion of the BPI family by duplication on human chromosome 20: characterization of the RY gene cluster in 20q11.21 encoding olfactory transporters/antimicrobial-like peptides. *Genomics.* 2003;82:172-184.

9. Cali G, Gentile F, Mogavero S, Pallante P, Nitsch R, Ciancia G, Ferraro A, Fusco A, Nitsch L. CDH16/Ksp-cadherin is expressed in the developing thyroid gland and is strongly down-regulated in thyroid carcinomas. *Endocrinology.* 2012;153:522-534.

10. Spinetti G, Fortunato O, Cordella D, Portararo P, Krankel N, Katare R, Sala-Newby GB, Richer C, Vincent MP, Alhenc-Gelas F, Tonolo G, Cherchi S, Emanueli C, Madeddu P. Tissue kallikrein is essential for invasive capacity of circulating proangiogenic cells. *Circ Res.* 2011;108:284-293.

11. Urbich C, Dimmeler S. Endothelial progenitor cells: characterization and role in vascular biology. *Circ Res.* 2004;95:343-353.

12. Urbich C, Dimmeler S. Endothelial progenitor cells functional characterization. *Trends Cardiovasc Med.* 2004;14:318-322.

13. Krankel N, Katare RG, Siragusa M, Barcelos LS, Campagnolo P, Mangialardi G, Fortunato O, Spinetti G, Tran N, Zacharowski K, Wojakowski W, Mroz I, Herman A, Manning Fox JE, MacDonald PE, Schanstra JP, Bascands JL, Ascione R, Angelini G, Emanueli C, Madeddu P. Role of kinin B2 receptor signaling in the recruitment of circulating progenitor cells with neovascularization potential. *Circ Res.* 2008;103:1335-1343.

14. Vecchione C, Patrucco E, Marino G, Barberis L, Poulet R, Aretini A, Maffei A, Gentile MT, Storto M, Azzolino O, Brancaccio M, Colussi GL, Bettarini U, Altruda F, Silengo L, Tarone G, Wymann MP, Hirsch E, Lembo G. Protection from angiotensin II-mediated vasculotoxic and hypertensive response in mice lacking PI3Kgamma. *J Exp Med.* 2005;201:1217-1228.

15. Vecchione C, Aretini A, Marino G, Bettarini U, Poulet R, Maffei A, Sbroggio M, Pastore L, Gentile MT, Notte A, Iorio L, Hirsch E, Tarone G, Lembo G. Selective Rac-1 inhibition protects from diabetes-induced vascular injury. *Circ Res.* 2006;98:218-225.

16. Zacchigna L, Vecchione C, Notte A, Cordenonsi M, Dupont S, Maretto S, Cifelli G, Ferrari A, Maffei A, Fabbro C, Braghetta P, Marino G, Selvetella G, Aretini A, Colonnese C, Bettarini U, Russo G, Soligo S, Adorno M, Bonaldo P, Volpin D, Piccolo S, Lembo G, Bressan GM. Emilin1 links TGF-beta maturation to blood pressure homeostasis. *Cell.* 2006;124:929-942.

17. Zhang Y, Chirmule N, Gao G, Wilson J. CD40 ligand-dependent activation of cytotoxic T lymphocytes by adeno-associated virus vectors in vivo: role of immature dendritic cells. *J Virol.* 2000;74:8003-8010.

18. Gao G, Vandenberghe LH, Alvira MR, Lu Y, Calcedo R, Zhou X, Wilson JM. Clades of Adeno-associated viruses are widely disseminated in human tissues. *J Virol.* 2004;78(12):6381-6388.

19. Auricchio A, Hildinger M, O'Connor E, Gao GP, Wilson JM. Isolation of highly infectious and pure adeno-associated virus type 2 vectors with a single-step gravity-flow column. *Hum Gene Ther.* 2001;12:71-76.

20. Doria M, Ferrara A, Auricchio A. AAV2/8 vectors purified from culture medium with a simple and rapid protocol transduce murine liver, muscle, and retina efficiently. *Hum Gene Ther Methods.* 2013;24:392-398.

21. Nelson DM, Wahlfors JJ, Chen L, Onodera M, Morgan RA. Characterization of diverse viral vector preparations, using a simple and rapid whole-virion dot-blot method. *Hum Gene Ther.* 1998;9:2401-2405.

22. R Development Core Team. *R: A language and environment for statistical computing*. Vienna, Austria: R Foundation for Statistical Computing; 2009.

23. Ferrario A, Villa F, Malovini A, Araniti F, Puca AA. The application of genetics approaches to the study of exceptional longevity in humans: potential and limitations. *Immun Ageing.* 2012;9:7.

24. Purcell S, Neale B, Todd-Brown K, Thomas L, Ferreira MA, Bender D, Maller J, Sklar P, de Bakker PI, Daly MJ, Sham PC. PLINK: a tool set for whole-genome association and population-based linkage analyses. *Am J Hum Genet.* 2007;81:559-575.

25. Schmittgen TD, Livak KJ. Analyzing real-time PCR data by the comparative C(T) method. *Nat Protoc.* 2008;3:1101-1108.

26. Tusher VG, Tibshirani R, Chu G. Significance analysis of microarrays applied to the ionizing radiation response. *Proc Natl Acad Sci U S A.* 2001;98:5116-5121.

27. Kiss T, Fayet-Lebaron E, Jady BE. Box H/ACA small ribonucleoproteins. *Mol Cell.*37:597-606.

28. de Jong OG, Verhaar MC, Chen Y, Vader P, Gremmels H, Posthuma G, Schiffelers RM, Gucek M, van Balkom BW. Cellular stress conditions are reflected in the protein and RNA content of endothelial cell-derived exosomes. *J Extracell Vesicles.*1.

29. Sekiguchi F, Nakahira T, Kawata K, Sunano S. Responses to endothelium-derived factors and their interaction in mesenteric arteries from Wistar-Kyoto and stroke-prone spontaneously hypertensive rats. *Clin Exp Pharmacol Physiol.* 2002;29:1066-1074.